

Supplementary Information

Crystal Structures, Red-shift Luminescent Properties And Iodide-anion

Recognition Of Four novel D-A Type Zn(II) Complexes

Jian-Biao Song^a, Pengfei Wang^a, Li Yan^b, Liang Hao^a, Maroof Ahmad Khan^a, Gui-lei Liu^c and Hui Li^{*a}

^a Key Laboratory of Clusters Science of Ministry of Education, School of Chemistry and Chemical Engineering, Beijing Institute of Technology, Beijing, 100081, P.R. China.

E-mail: lihui@bit.edu.cn; Fax: +86 10 68912667.

^b Analysis and Testing Center, Beijing Institute of Technology, Beijing, 100081, P. R. China.

E-mail: 626828807@qq.com.

^c National Research Center for Geoanalysis, Beijing 100037, P. R. China.

Email: liuguilei2008@163.com; Tel: 86-10-68999561.

Content

1. Infrared spectrum of complexes 1, 2, 3 and 4	3
2. ¹ H NMR spectrum of complexes 1, 2, 3 and 4	5
3. Single crystal structures and crystallographic data of complexes 1, 2, 3 and 4	7
4. X-ray powder diffraction of complexes 1, 2, 3 and 4	15
5. Thermal gravity analysis of complexes 1, 2, 3 and 4	17
6. UV-Vis spectra of complexes 1, 2, 3 and 4 in different kinds of solutions.....	19
7. Fluorescence spectra, quantum yield and lifetime of complexes 1, 2, 3 and 4	21
8. CIEE properties of complexes 1, 2, 3 and 4	24
9. DFT and TD-DFT Computations of the ligands of complexes 1, 2, 3 and 4	25
10. UV-vis titration of complexes 1, 2, 3 and 4 with F ⁻ , Cl ⁻ and Br ⁻ in THF.....	27
11. Fluorescence titration of complexes 1, 2, 3 and 4 with F ⁻ , Cl ⁻ and Br ⁻ in THF.....	33
12. Iodide recognition of complexes 1, 2, 3 and 4 in THF.....	39
13. Benesi-Hilderbrand and Job's plot curve of complexes 1, 2, 3 and 4 with I ⁻ monitored with UV-Vis spectra.....	40

1. Infrared Radiation spectrum of complexes **1**, **2**, **3** and **4**

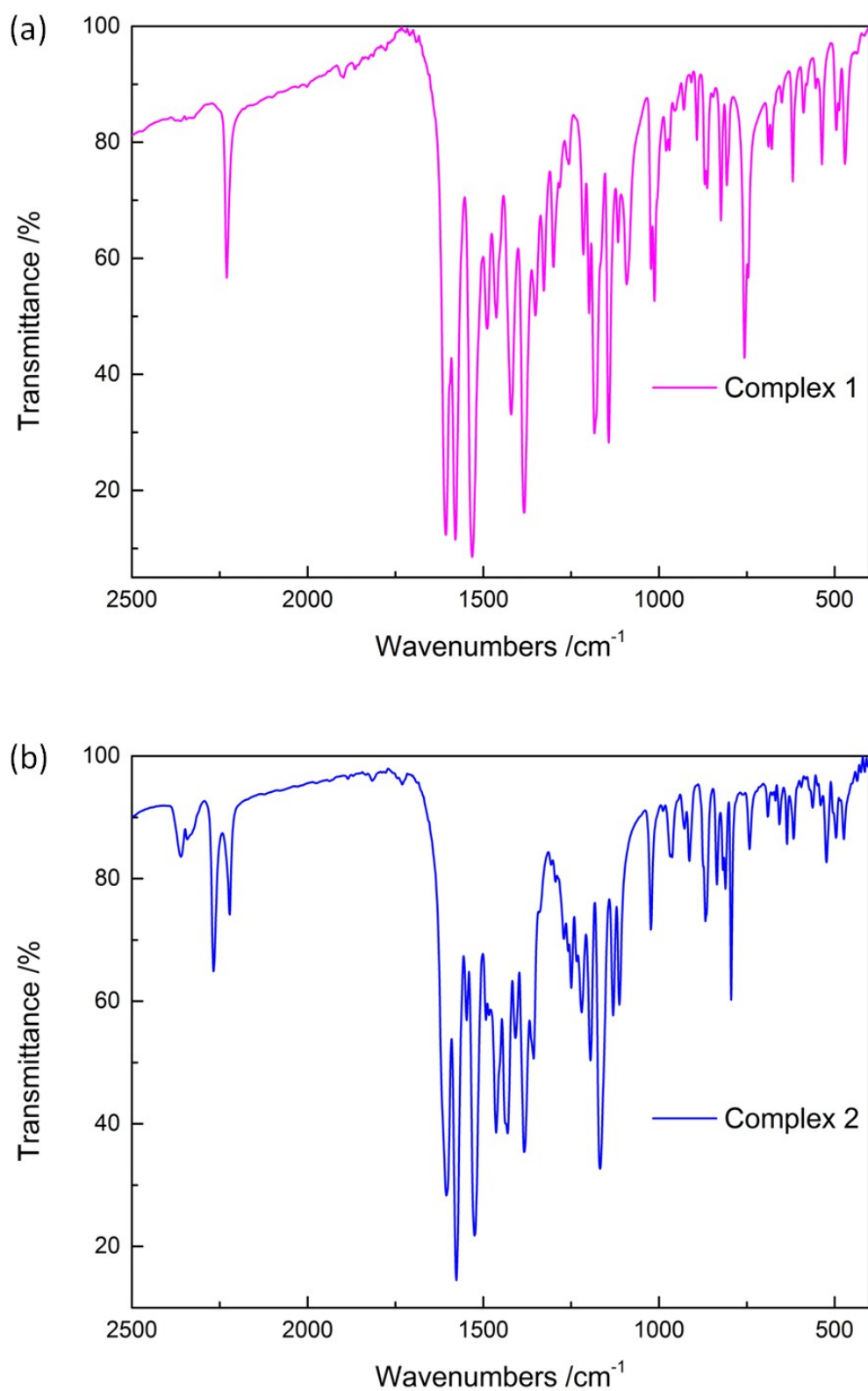


Fig. S1 IR spectrum of **1** (a) and **2** (b).

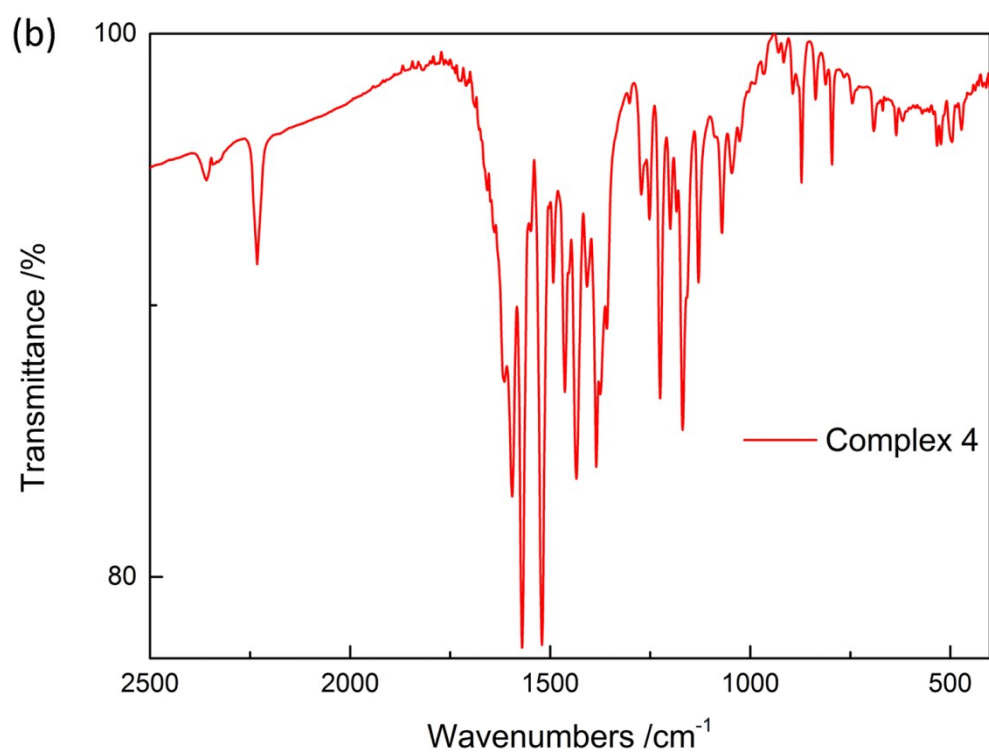
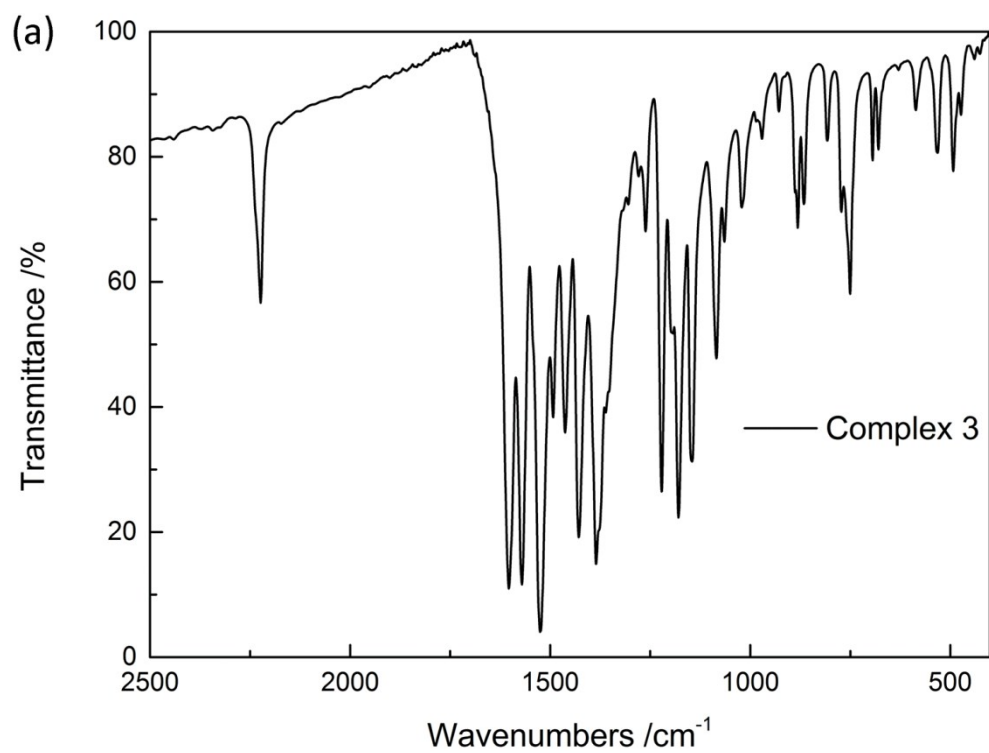


Fig. S2 IR spectrum of **3** (a) and **4** (b).

2. ^1H NMR spectrum of complexes **1**, **2**, **3** and **4**

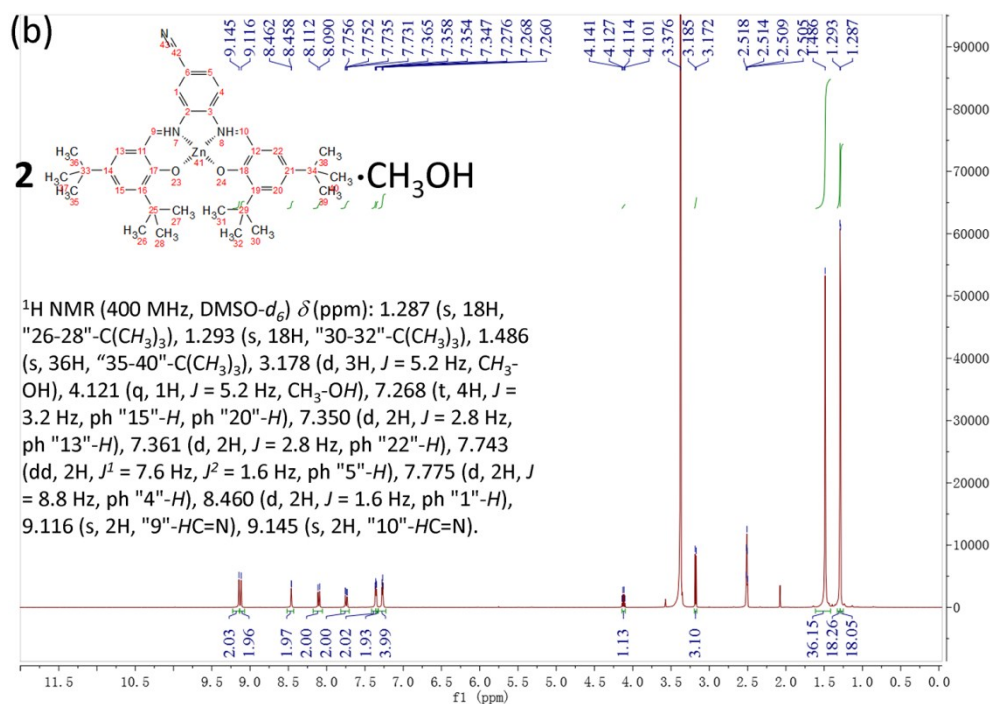
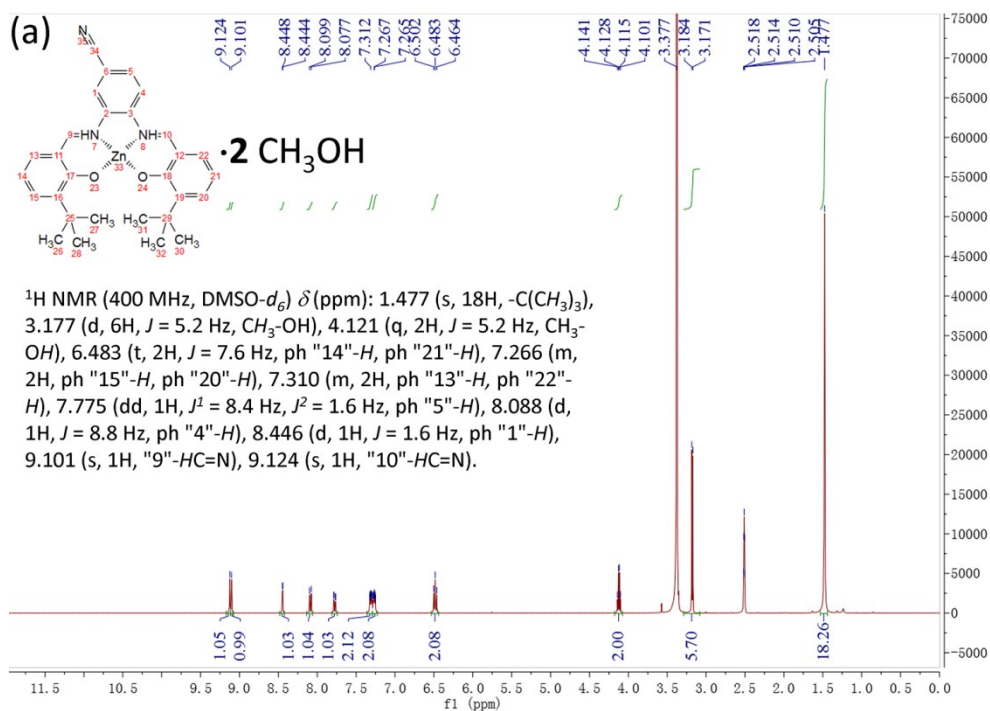


Fig. S3 ^1H NMR spectrum (400 MHz, 298K) of complexes **1** (a) and **2** (b) in $\text{DMSO}-d_6$.

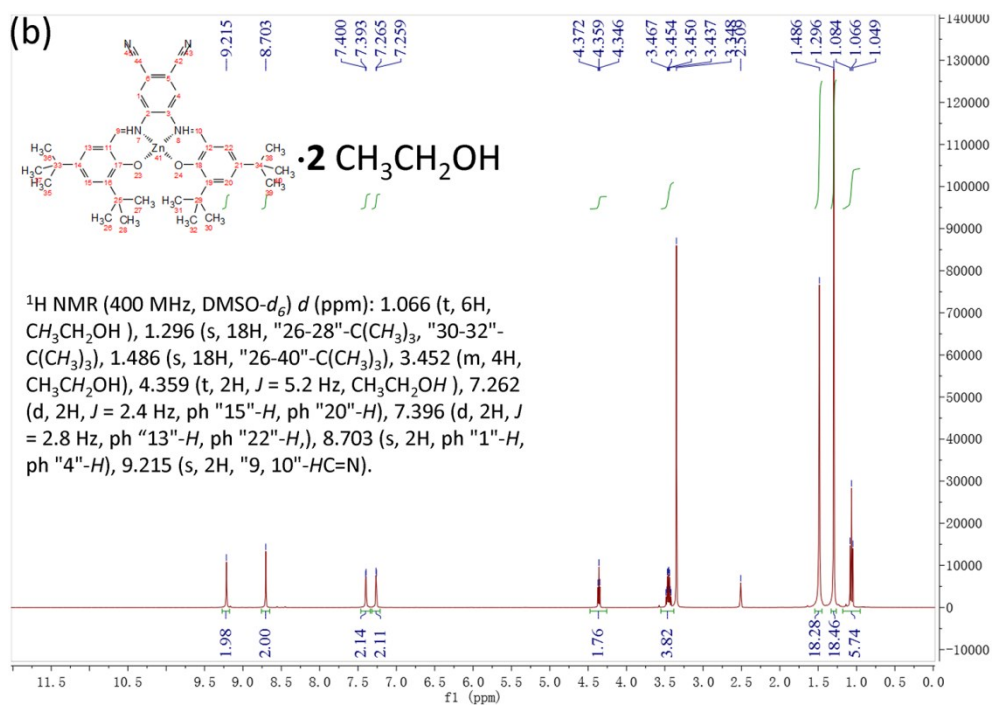
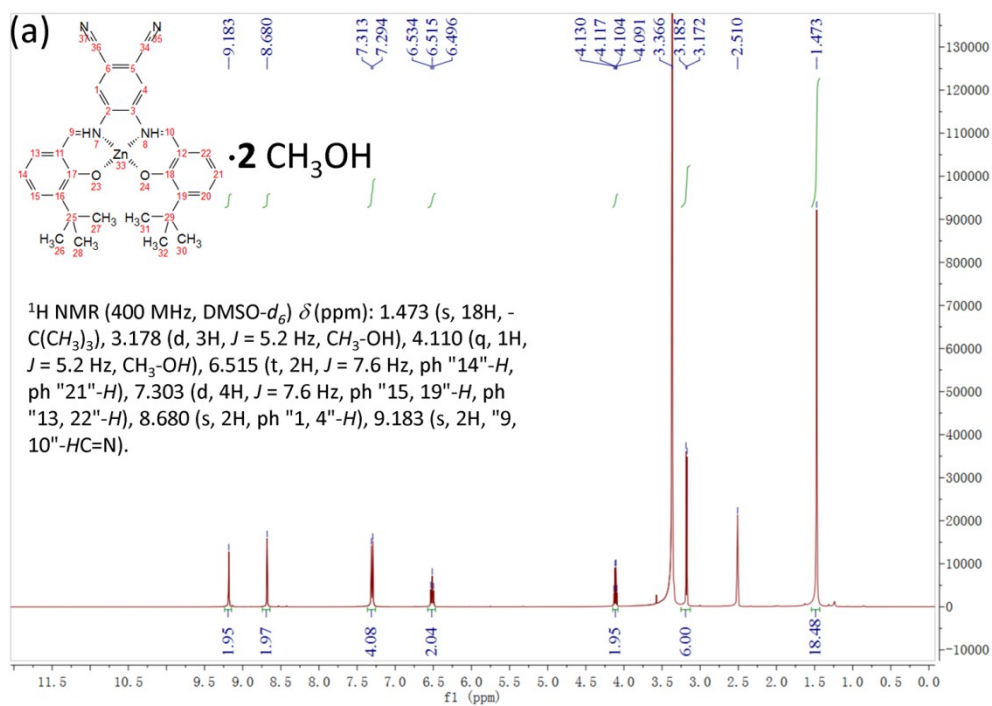


Fig. S4 ^1H NMR spectrum (400 MHz, 298K) of complexes 3 (a) and 4 (b) in $\text{DMSO}-d_6$.

3. Single crystal structures and crystallographic data of complexes 1, 2, 3 and 4

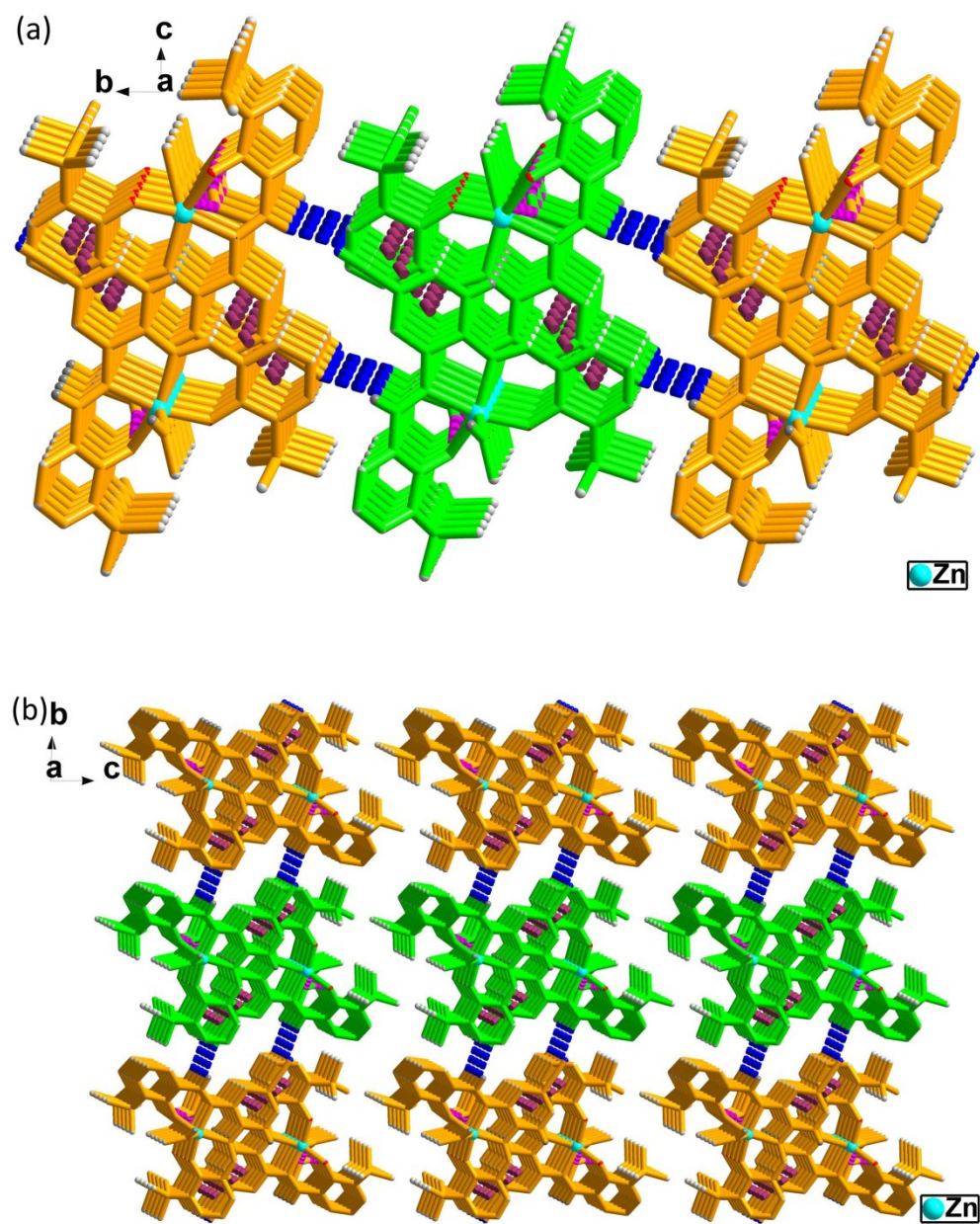


Fig. S5 (a) Picture of the 2D layer of complex 1 assembly based on a nonclassical H-bonding (C8-H8A...N3, 2.530 Å, 3.441 Å, 166.53°) from *a* axis; (b) the 3D stacking picture formed *via* van der Waals interactions viewed down from *a* axis (hydrogen atoms without forming H-bonds are omitted for clarity).

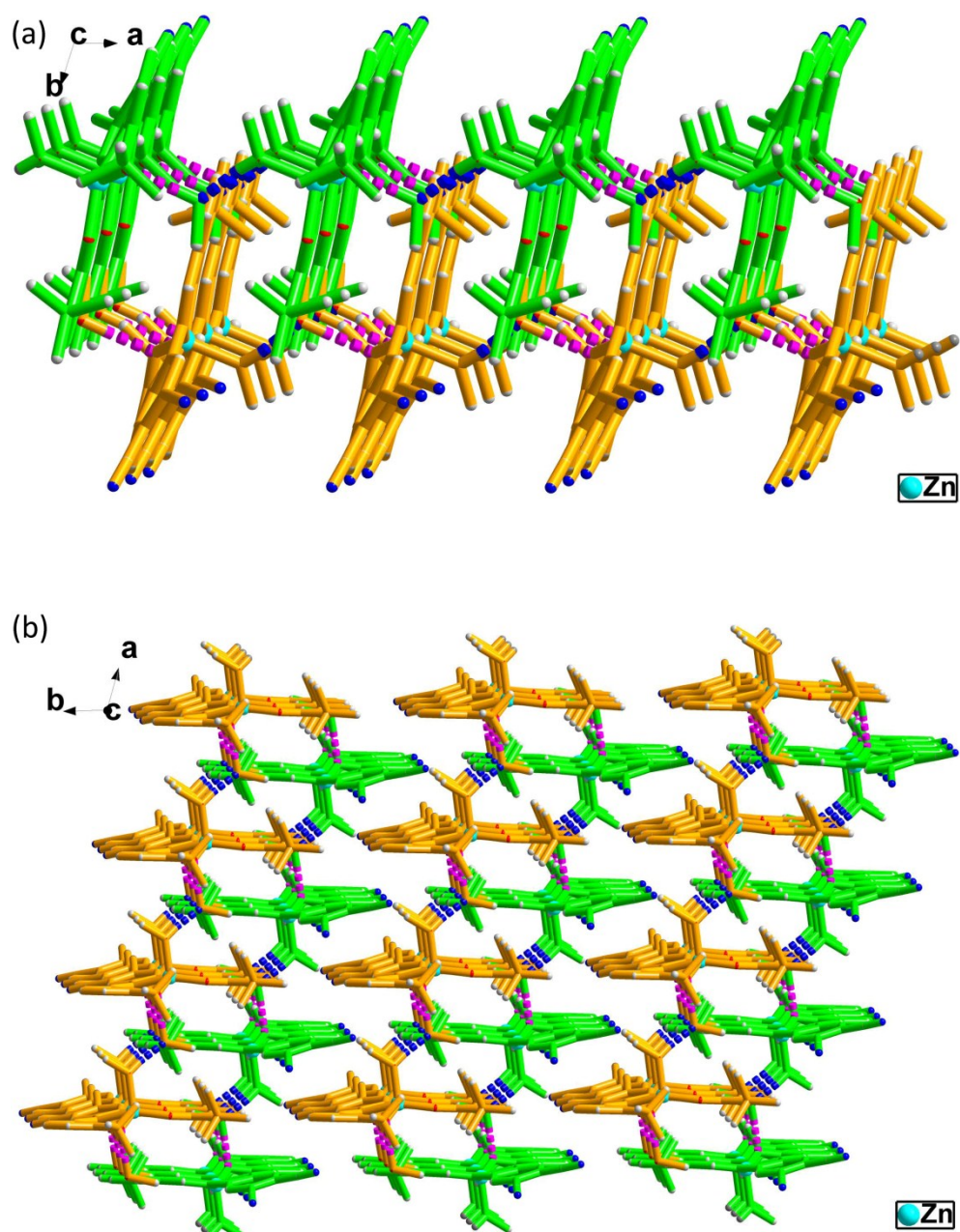


Fig. S6 (a) Picture of the 2D layer of complex **3** assembly based on Van der Waals' force from *c* axis; (b) the 3D stacking picture also formed *via* van der waals interactions viewed down (d) from *c* axis (hydrogen atoms without forming H-bonds are omitted for clarity).

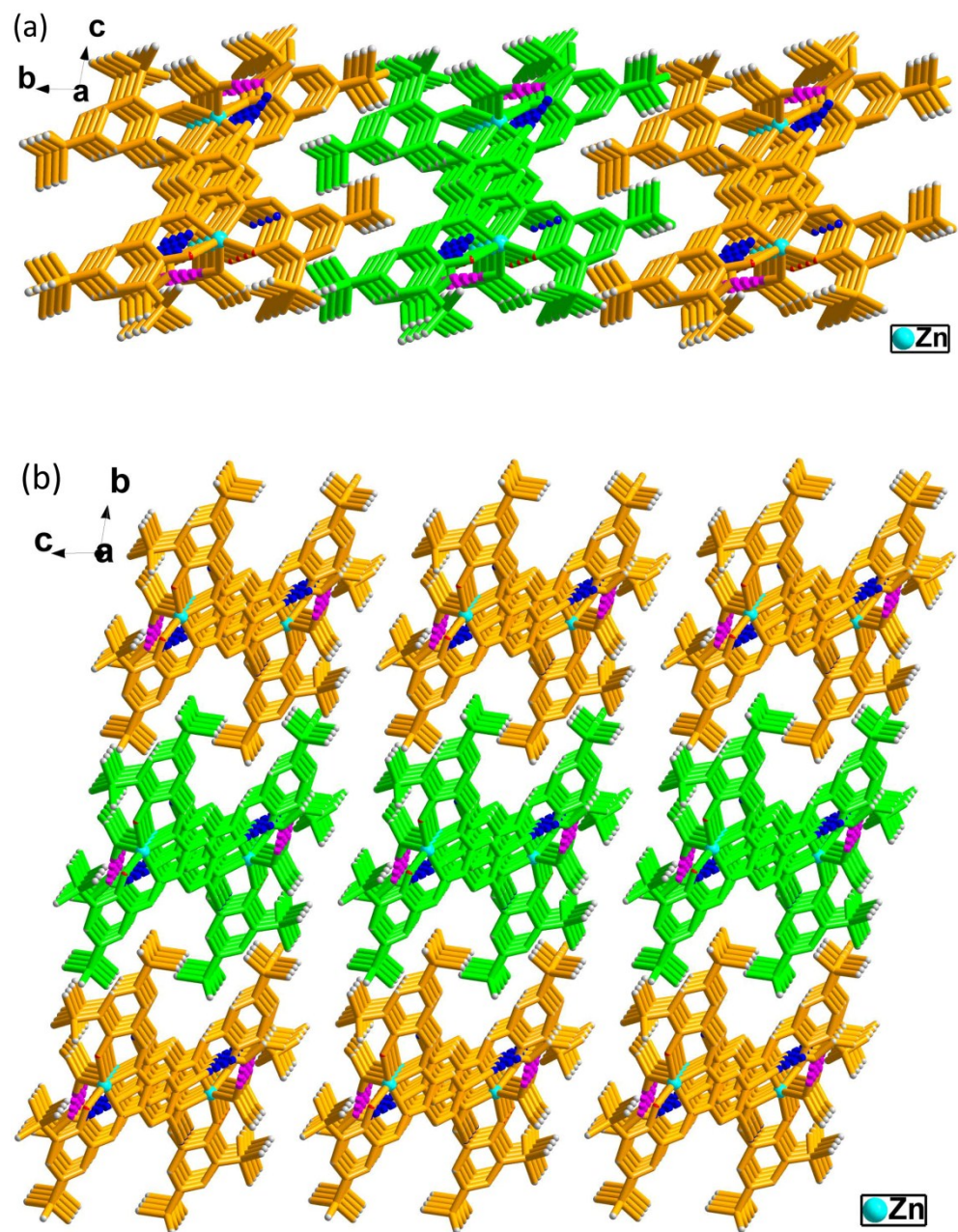


Fig. S7 (a) Picture of the 2D layer of complex 4 assembly based on Van der Waals' force from *a* axis; (b) the 3D stacking picture also formed *via* van der Waals interactions viewed down (d) from *a* axis (hydrogen atoms without forming H-bonds are omitted for clarity).

Table S1 Crystallographic data for **1**, **2**, **3** and **4**.

Complexes	1	2	3	4
Formula	C ₃₁ H ₃₇ N ₃ O ₄ Zn	C ₇₅ H ₉₄ N ₆ O ₅ Zn ₂	C ₃₂ H ₃₆ N ₄ O ₄ Zn	C ₄₂ H ₅₆ N ₄ O ₄ Zn
<i>M</i> /mol ⁻¹	581.00	1290.30	606.02	746.27
<i>T</i> /K	296(2)	296(2)	296(2)	296(2)
Crystal system	Triclinic	Orthorhombic	Triclinic	Triclinic
Space group	<i>P</i> -1	<i>Pbca</i>	<i>P</i> -1	<i>P</i> -1
<i>a</i> /Å	7.3914(10)	31.102(6)	7.3811(13)	10.8277(9)
<i>b</i> /Å	11.1728(15)	13.649(3)	13.9023(18)	13.0401(9)
<i>c</i> /Å	18.077(2)	33.418(7)	16.664(2)	15.7196(13)
α /°	88.210(3)	90.00	99.06(3)	96.621(2)
β /°	79.092(4)	90.00	102.13(2)	101.707(3)
γ /°	87.909(5)	90.00	104.723(18)	102.6800(10)
<i>V</i> /Å ³	1464.5(3)	14186(5)	1576.2(5)	2090.5(3)
<i>Z</i>	2	8	2	2
F(000)	612	5488	636	796
ρ (calculated)/g·cm ⁻³	1.318	1.208	1.277	1.186
μ (Mo Ka)/mm ⁻¹	0.878	0.729	0.820	0.630
2 θ range/°	2.13-26.99	1.38-25.32	1.55-24.98	2.498-28.378
Reflns collected	16333	89615	8602	41720
Independent reflns	6359	12890	5389	10359
<i>R</i> _{int}	0.0467	0.1432	0.1279	0.0877
Data/restraints/parameters	6359/0/354	12890/108/794	5389/0/372	10359/78/497
<i>R</i> ₁ ^a [<i>I</i> >2 σ (<i>I</i>)]	0.0667	0.0653	0.1108	0.0567
<i>wR</i> ₂ ^b [<i>I</i> >2 σ (<i>I</i>)]	0.1938	0.1644	0.1782	0.1150
<i>R</i> ₁ (all data)	0.0908	0.1543	0.2595	0.1201
<i>wR</i> ₂ (all data)	0.2137	0.2058	0.2209	0.1391
Goodness-of-fit on <i>F</i> ²	1.044	1.025	1.101	1.041
$\Delta\rho_{\max,\min}$ /e Å ⁻³	1.810, -0.521	0.526, -0.739	1.022, -1.010	0.502, -0.412

$$^a R_1 = \frac{\sum ||F_o| - |F_c||}{\sum |F_o|}; \quad ^b wR_2 = \frac{\sum [w(F_o^2 - F_c^2)^2]}{\sum [w(F_o^2)^2]}^{1/2}$$

Table S2. Selected bond distances (Å) and angles (°) for **1**

Zn1—O3	1.937 (3)	O3—Zn1—O1	100.14 (14)
Zn1—O2	2.002 (3)	O2—Zn1—O1	101.92 (13)
Zn1—N1	2.078 (3)	N1—Zn1—O1	104.38 (14)
Zn1—N2	2.080 (3)	N2—Zn1—O1	94.79 (13)
Zn1—O1	2.087 (3)	C14—O2—Zn1	121.3 (2)
O3—Zn1—O2	97.54 (12)	C24—O3—Zn1	129.3 (3)
O3—Zn1—N1	90.77 (13)	C8—N2—Zn1	120.8 (3)
O2—Zn1—N1	150.52 (13)	C2—N2—Zn1	114.7 (3)
O3—Zn1—N2	163.46 (14)	C31—O1—Zn1	119.9 (3)
O2—Zn1—N2	86.22 (12)	C26—N1—Zn1	121.6 (3)
N1—Zn1—N2	78.57 (13)	C1—N1—Zn1	115.1 (3)

\

Table S3. Selected bond distances (Å) and angles (°) for **2**.

Zn1—O1	1.924 (4)	C24—O2—Zn1	118.7 (3)
Zn1—O2	1.973 (3)	C10—O1—Zn1	131.2 (4)
Zn1—N1	2.047 (4)	C8—N1—Zn1	124.0 (4)
Zn1—N2	2.083 (4)	C6—N1—Zn1	114.6 (3)
Zn1—N6i	2.094 (5)	C22—N2—Zn1	121.4 (3)
Zn2—O3	1.937 (3)	C5—N2—Zn1	113.8 (3)
Zn2—O4	1.942 (4)	C1—N6—Zn1ii	168.6 (5)
Zn2—O5	2.075 (4)	O4—Zn2—N3	151.28 (16)
Zn2—N3	2.077 (4)	O5—Zn2—N3	103.53 (14)
Zn2—N4	2.079 (4)	O3—Zn2—N4	160.83 (16)
O1—Zn1—O2	98.98 (15)	O4—Zn2—N4	88.41 (15)
O1—Zn1—N1	90.50 (16)	O5—Zn2—N4	97.73 (15)
O2—Zn1—N1	148.42 (16)	N3—Zn2—N4	78.79 (16)
O1—Zn1—N2	166.54 (17)	C63—O3—Zn2	132.4 (3)
O2—Zn1—N2	86.33 (15)	C47—O4—Zn2	131.8 (3)
N1—Zn1—N2	78.83 (16)	C61—N3—Zn2	123.6 (3)
O1—Zn1—N6i	99.57 (18)	C43—N3—Zn2	113.6 (3)
O2—Zn1—N6i	98.04 (16)	C45—N4—Zn2	123.2 (4)
N1—Zn1—N6i	110.05 (18)	C42—N4—Zn2	113.5 (3)
N2—Zn1—N6i	91.85 (18)	C60—O5—Zn2	127.0 (4)

Symmetry codes: (i) $-x+1, y, -z+1/2$.

Table S4. Selected bond distances (Å) and angles (°) for **3**

Zn1—O2	1.965 (5)	O2—Zn1—N2	157.4 (2)
Zn1—O1	1.986 (6)	O1—Zn1—N2	85.8 (2)
Zn1—O3	2.033 (6)	O3—Zn1—N2	99.6 (3)
Zn1—N1	2.071 (7)	N1—Zn1—N2	79.6 (3)
Zn1—N2	2.104 (6)	C11—O1—Zn1	125.6 (5)
O2—Zn1—O1	94.9 (2)	C22—O2—Zn1	133.5 (5)
O2—Zn1—O3	102.0 (3)	C9—N2—Zn1	124.9 (5)
O1—Zn1—O3	105.6 (3)	C8—N2—Zn1	113.1 (5)
O2—Zn1—N1	89.3 (3)	C32—O3—Zn1	128.8 (6)
O1—Zn1—N1	150.8 (2)	C20—N1—Zn1	124.5 (5)
O3—Zn1—N1	101.8 (3)	C7—N1—Zn1	113.5 (5)

Table S5. Selected bond distances (Å) and angles (°) for **4**

Zn1—O2	1.935 (2)	O2—Zn1—N2	163.02 (10)
Zn1—O3	1.942 (2)	O3—Zn1—N2	88.35 (8)
Zn1—N1	2.073 (2)	N1—Zn1—N2	78.78 (9)
Zn1—O1	2.073 (2)	O1—Zn1—N2	94.40 (10)
Zn1—N2	2.081 (2)	C15—O3—Zn1	127.32 (19)
O2—Zn1—O3	96.93 (9)	C1—N1—Zn1	124.08 (19)
O2—Zn1—N1	89.75 (9)	C33—N1—Zn1	113.36 (17)
O3—Zn1—N1	153.69 (10)	C14—N2—Zn1	122.94 (19)
O2—Zn1—O1	100.26 (11)	C32—N2—Zn1	113.13 (17)
O3—Zn1—O1	101.68 (10)	C7—O2—Zn1	132.05 (19)
N1—Zn1—O1	102.11 (10)	C41—O1—Zn1	129.9 (6)

Table S6. Selected H-bonding distances (Å) and angles (°) for **1**.

D-H	d(D-H)	d(H···A)	∠DHA	d(D···A)	A	Symmetry
O1-H1A	0.821	1.994	145.09	2.709	O4	$[x + 1, y, z]$
O4-H4	0.820	1.910	166.75	2.715	O2	
C8-H8A	0.930	2.530	166.53	3.441	N3	$[-x + 2, -y, -z + 1]$

Table S7. Selected H-bonding distances (Å) and angles (°) for **2**.

D-H	d(D-H)	d(H···A)	∠DHA	d(D···A)	A	Symmetry
O5-H5D	0.850	1.833	159.25	2.645	O2	

Table S8. Selected H-bonding distances (Å) and angles (°) for **3**.

D-H	d(D-H)	d(H···A)	∠DHA	d(D···A)	A	Symmetry
O3-H3	0.854	1.828	172.38	2.676	O4	
O4-H4	0.820	1.907	173.75	2.724	O1	$[x + 1, y, z]$

Table S9. Selected H-bonding distances (Å) and angles (°) for **4**.

D-H	d(D-H)	d(H···A)	∠DHA	d(D···A)	A	Symmetry
O1-H1	0.782	1.922	167.78	2.692	O4	
O4-H4A	0.820	2.118	153.78	2.877	N3	$[-x + 2, -y + 1, -z + 1]$

4. X-ray powder diffraction of complexes **1**, **2**, **3** and **4**.

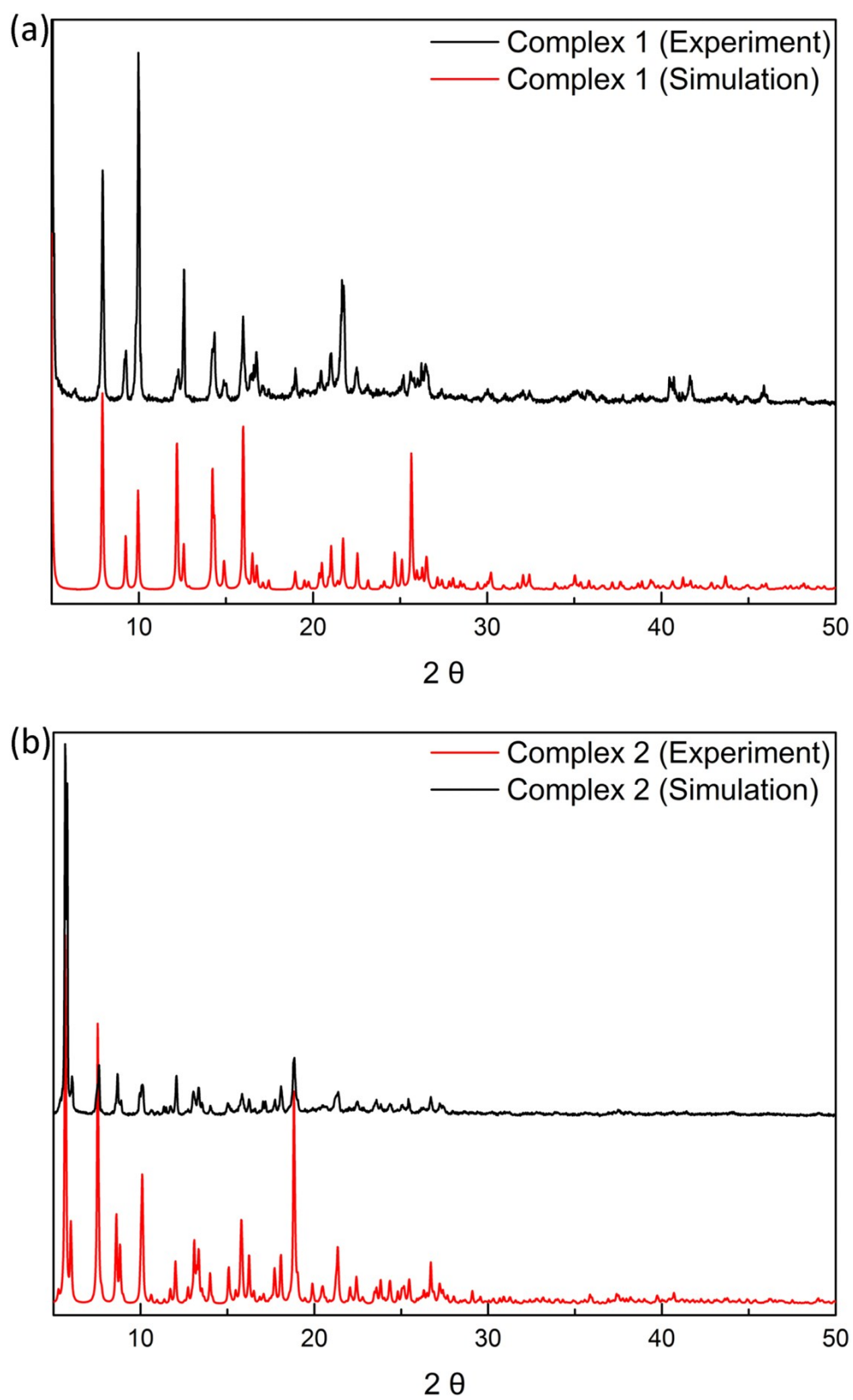


Fig. S8 PXRD patterns show the comparison between the experimental value and calculated ones for **1** (a) and **2** (b).

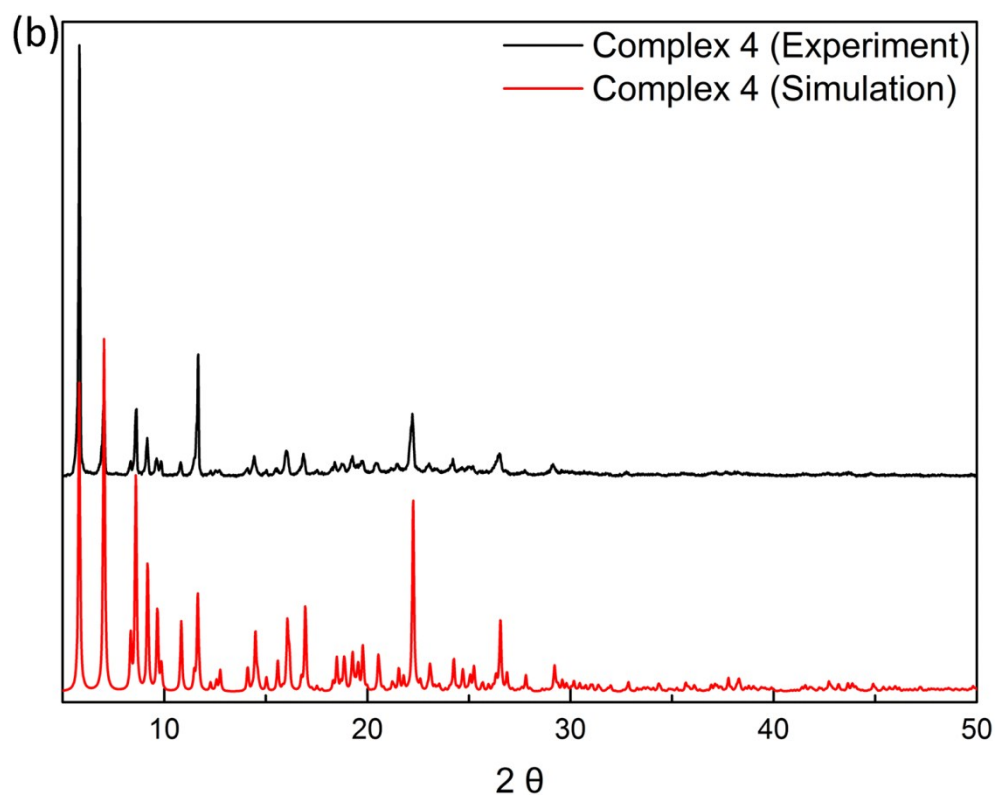
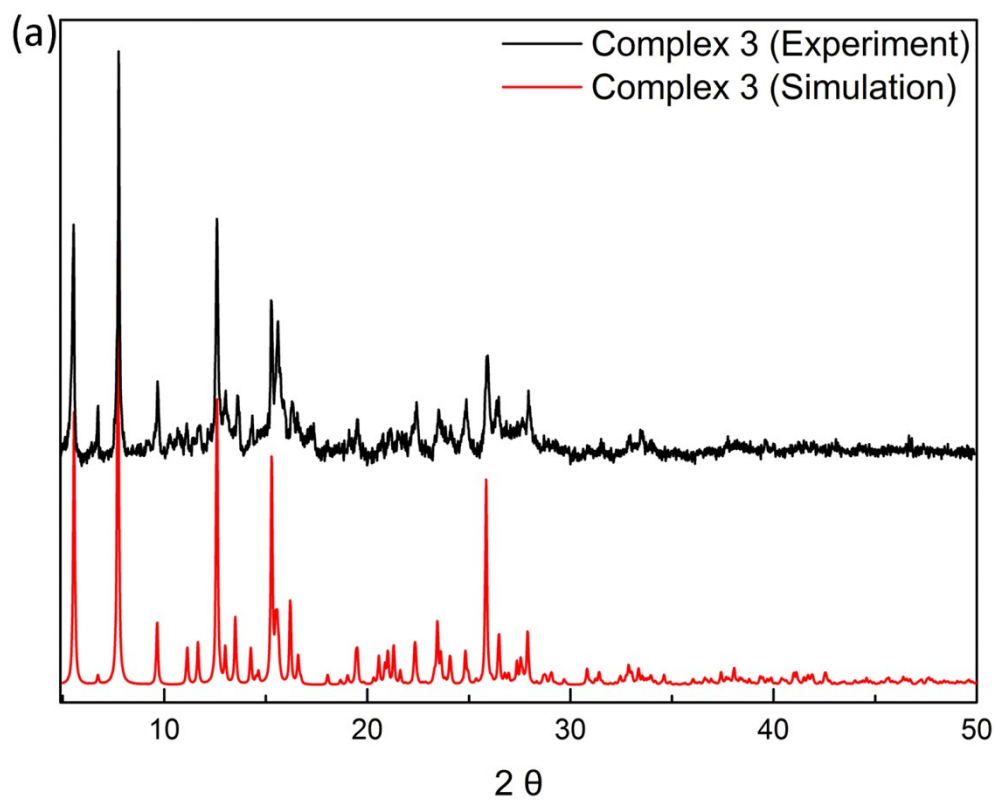


Fig. S9 PXRD patterns show the comparison between the experimental value and calculated ones for **3** (a) and **4** (b).

5. Thermal gravity analysis of complexes 1, 2, 3 and 4

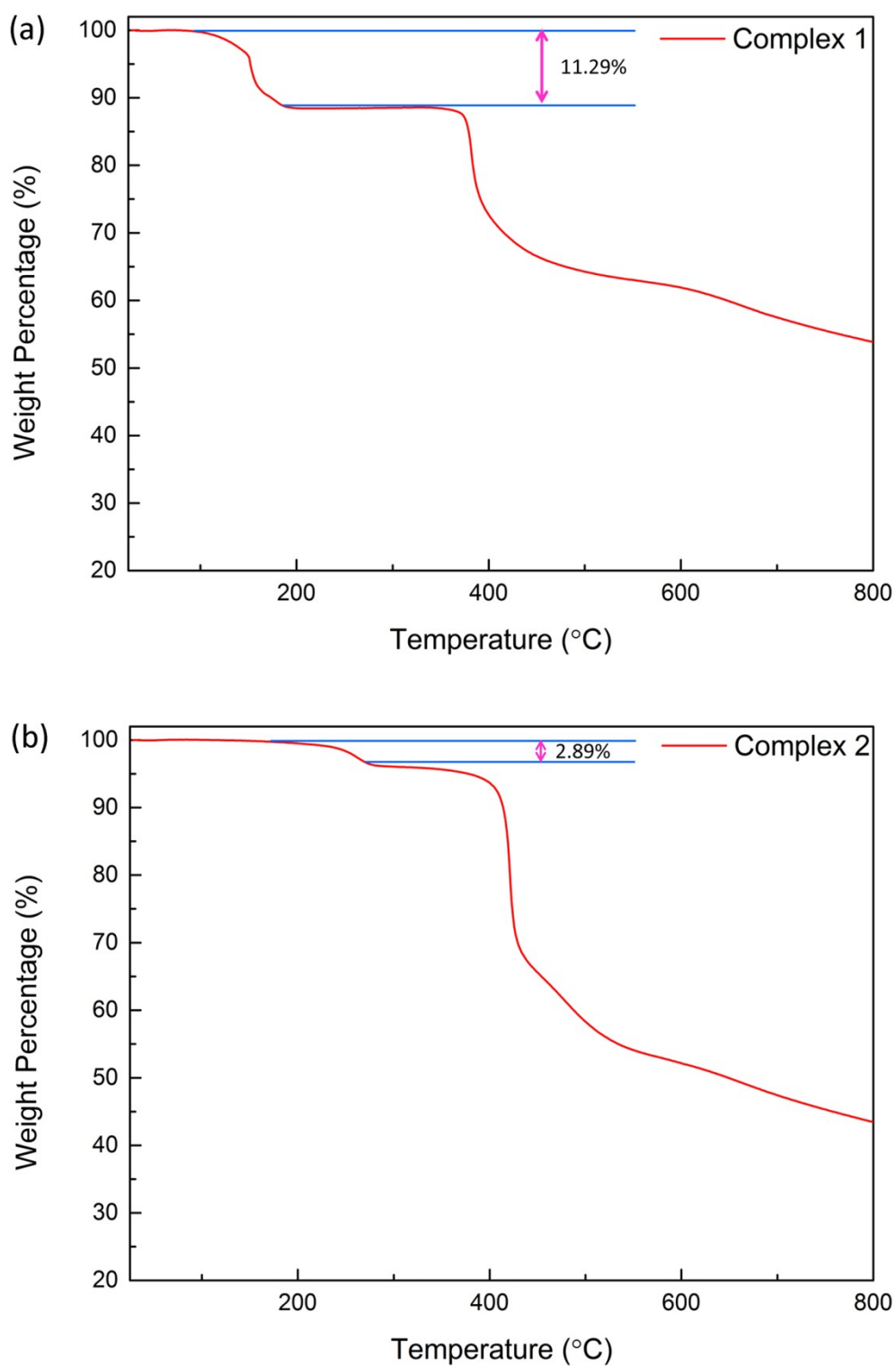


Fig. S10 TGA curves of complexes 1 (a) and 2 (b).

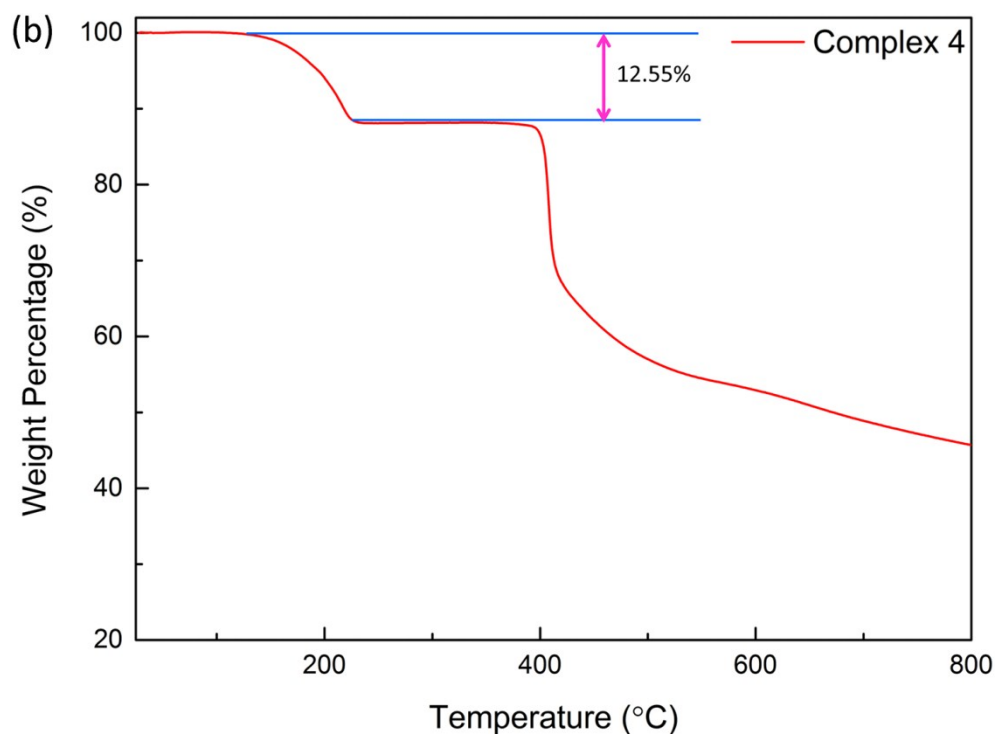
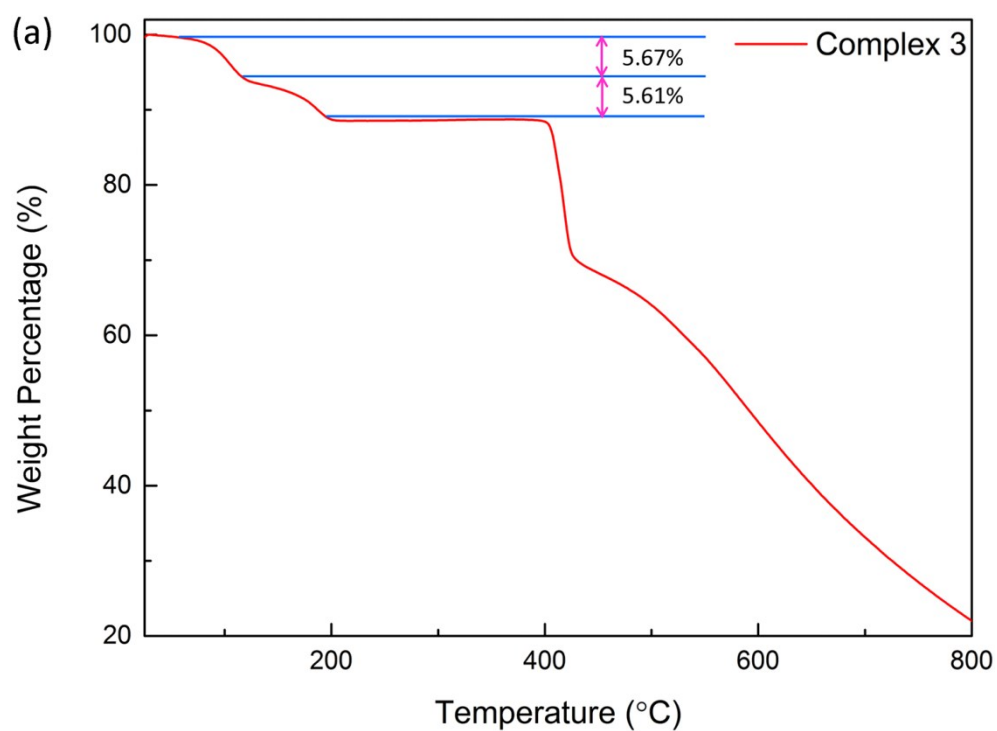


Fig. S11 TGA curves of complexes **3** (a) and **4** (b).

6. UV-Vis spectra of complexes **1**, **2**, **3** and **4** in different kinds of solutions

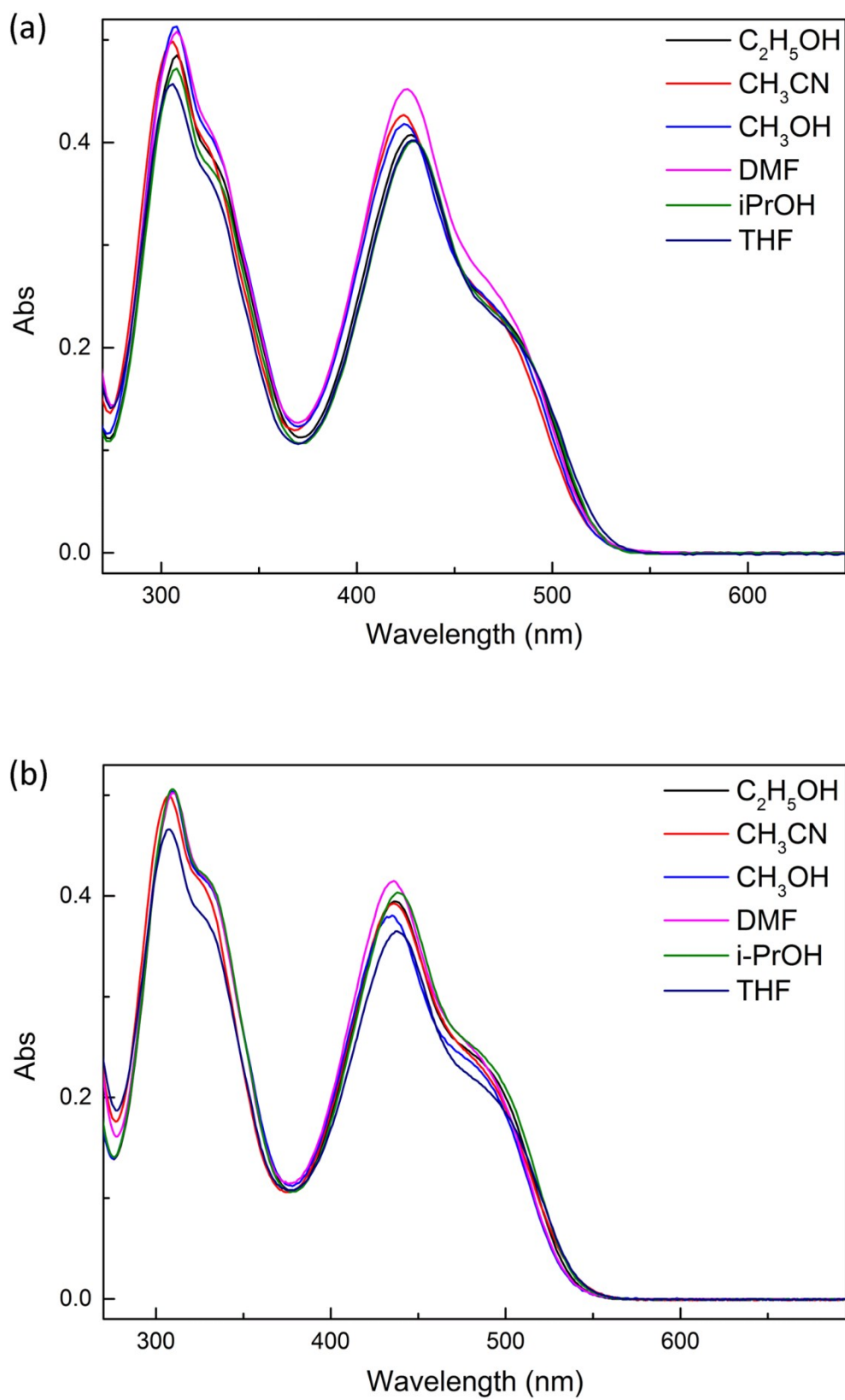


Fig. S12 UV-Vis spectra of complexes **1** (2.5 × 10⁻⁵ mol·L⁻¹) (a) and **2** (2.5 × 10⁻⁵ mol·L⁻¹) (b) with different solutions.

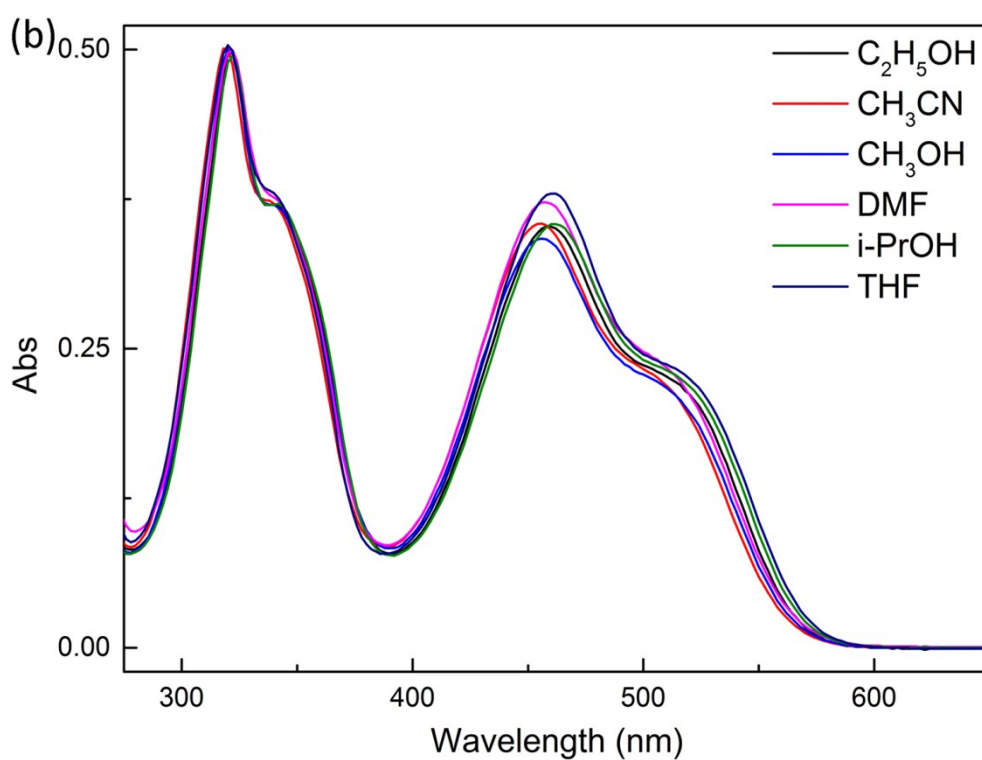
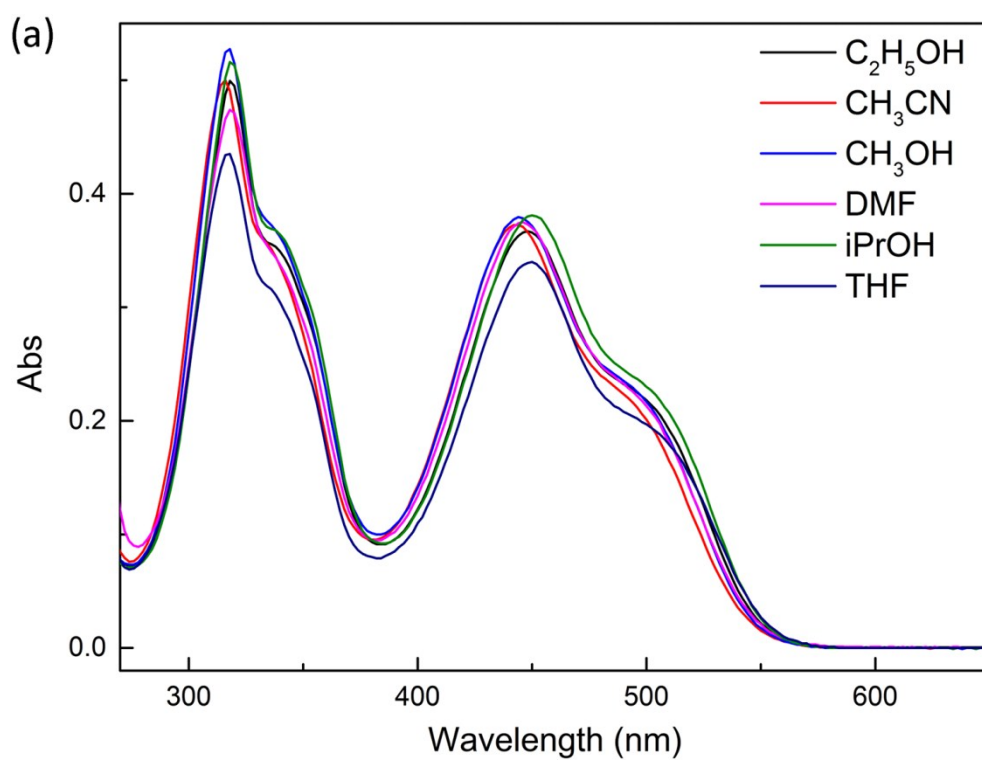


Fig. S13 UV-Vis spectra of complexes **3** ($2.5 \times 10^{-5} \text{ mol} \cdot \text{L}^{-1}$) (a) and **4** ($2.5 \times 10^{-5} \text{ mol} \cdot \text{L}^{-1}$) (b) with different solutions.

7. Fluorescence spectra, quantum yield and lifetime of complexes **1**, **2**, **3** and **4**

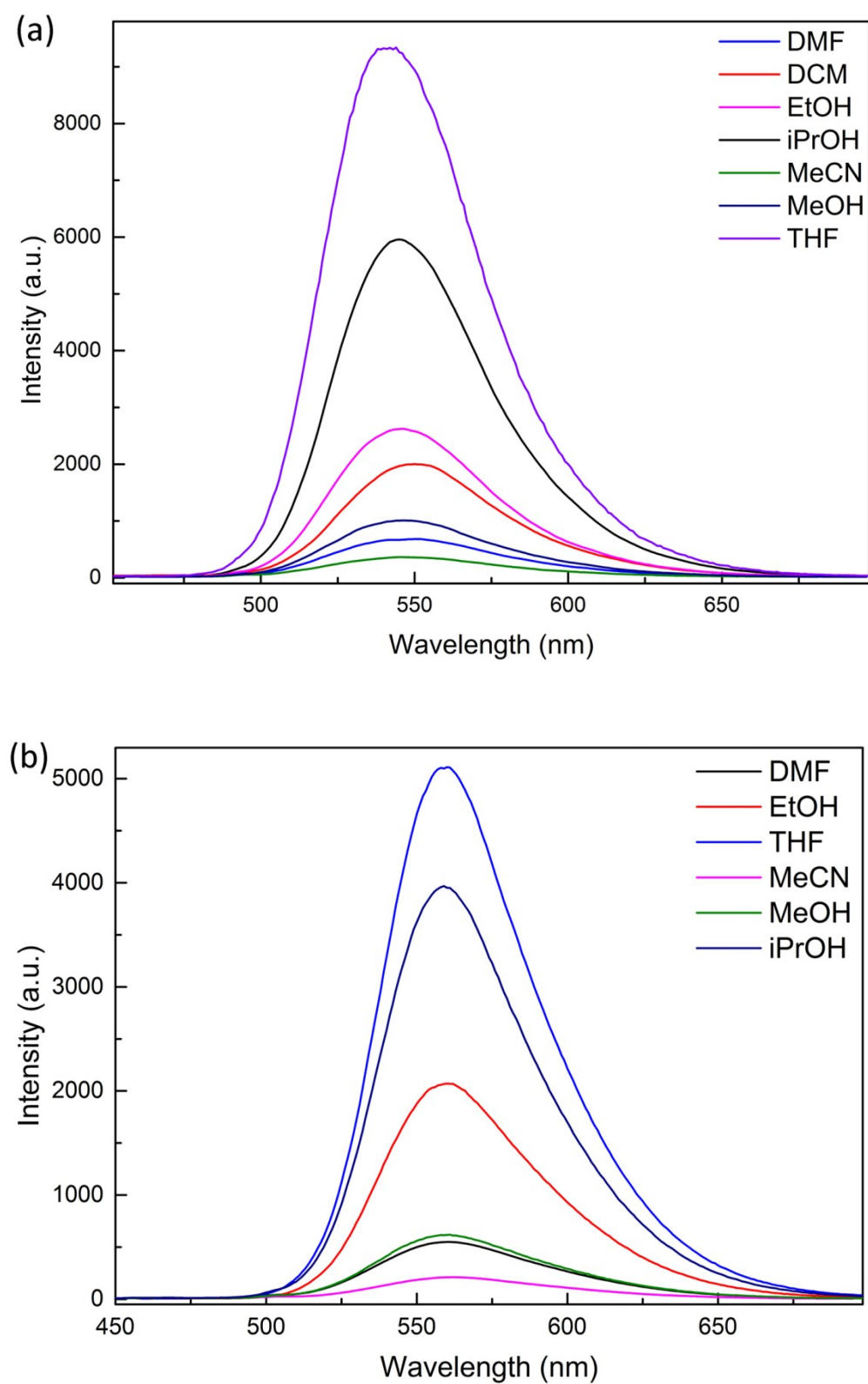


Fig. S14 (a) Fluorescence ($\lambda_{\text{exc}} = 445 \text{ nm}$) spectra of **1** ($2.5 \times 10^{-5} \text{ mol} \cdot \text{L}^{-1}$) (a) and **2** ($2.5 \times 10^{-5} \text{ mol} \cdot \text{L}^{-1}$) (b) with different kinds of solutions.

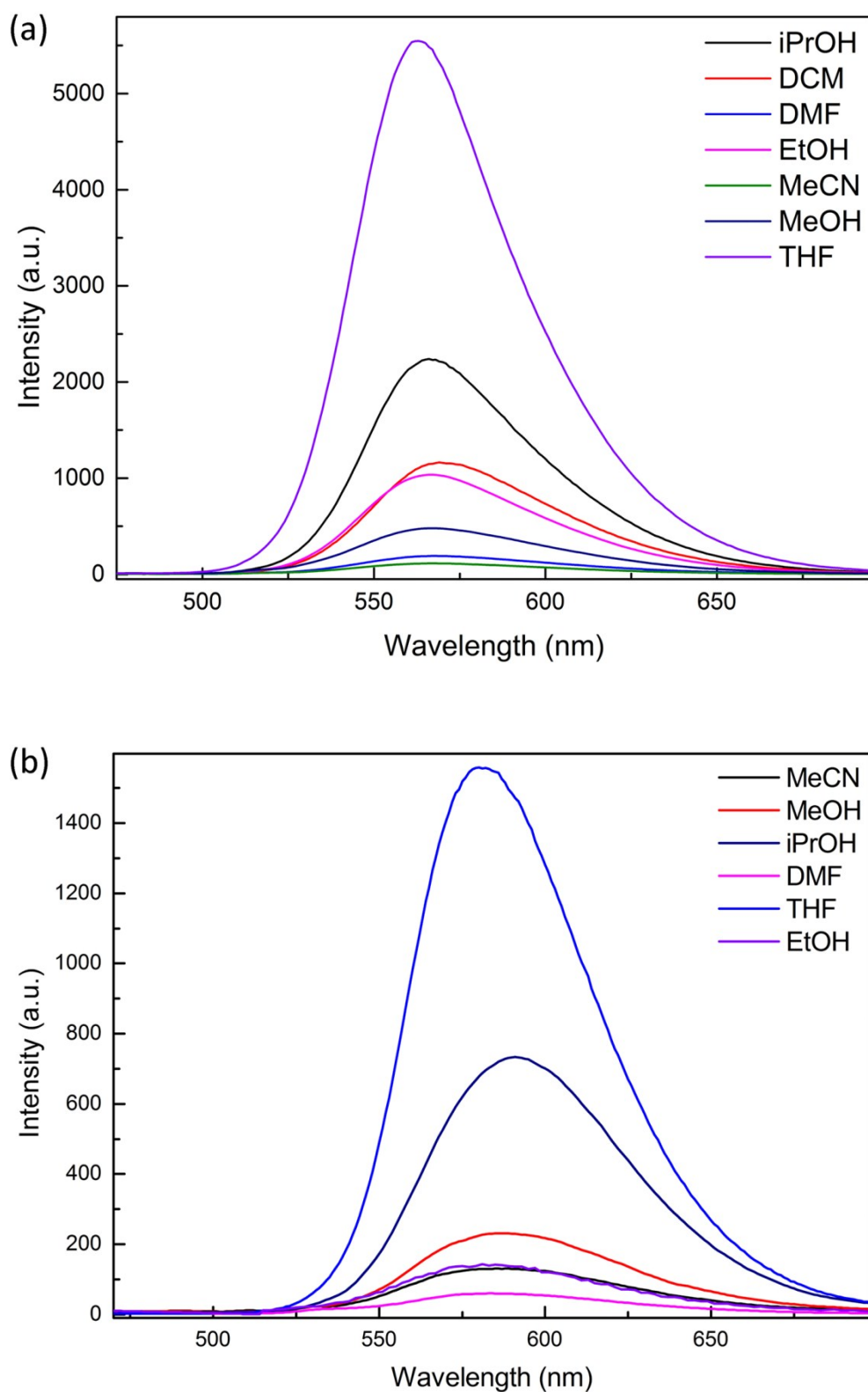


Fig. S15 (a) Fluorescence ($\lambda_{\text{exc}} = 445 \text{ nm}$) spectra of **3** ($2.5 \times 10^{-5} \text{ mol} \cdot \text{L}^{-1}$) (a) and **4** ($2.5 \times 10^{-5} \text{ mol} \cdot \text{L}^{-1}$) (b) with different kinds of solutions.

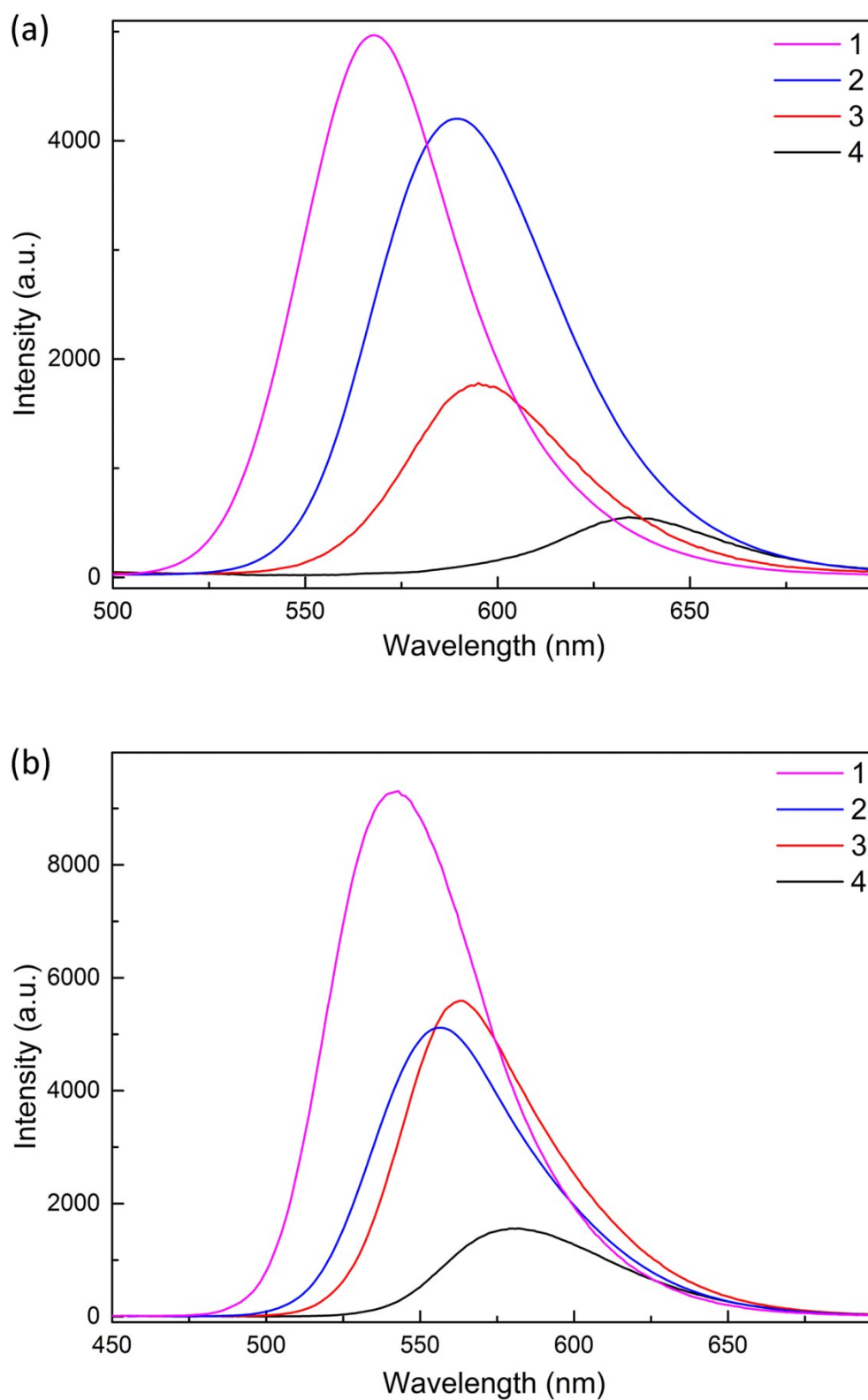


Fig. S16 (a) Solid state fluorescence spectra ($\lambda_{exc} = 385$ nm) of complexes **1**, **2**, **3** and **4**; (b) Fluorescence spectra ($\lambda_{exc} = 445$ nm) of complexes **1**, **2**, **3** and **4** (concentration of every of them is $2.5 \times 10^{-5} \text{ mol} \cdot \text{L}^{-1}$) in THF.

Table S10 The absolute solid state fluorescence quantum yield and lifetime of **1**, **2**, **3** and **4**

	1	2	3	4
Absolute quantum yield (Φ /%)	73.24	50.97	10.50	4.61
Lifetime (t/ns)	0.702	1.198	0.606	0.449

Table S11 The absolute fluorescence quantum yield and lifetime of **1**, **2**, **3** and **4** in THF solution

	1	2	3	4
Absolute quantum yield (Φ /%)	8.25	4.27	6.04	3.08
Lifetime (t/ns)	1.023	0.861	0.971	0.747

8. CIEE properties of complexes **1**, **2**, **3** and **4**

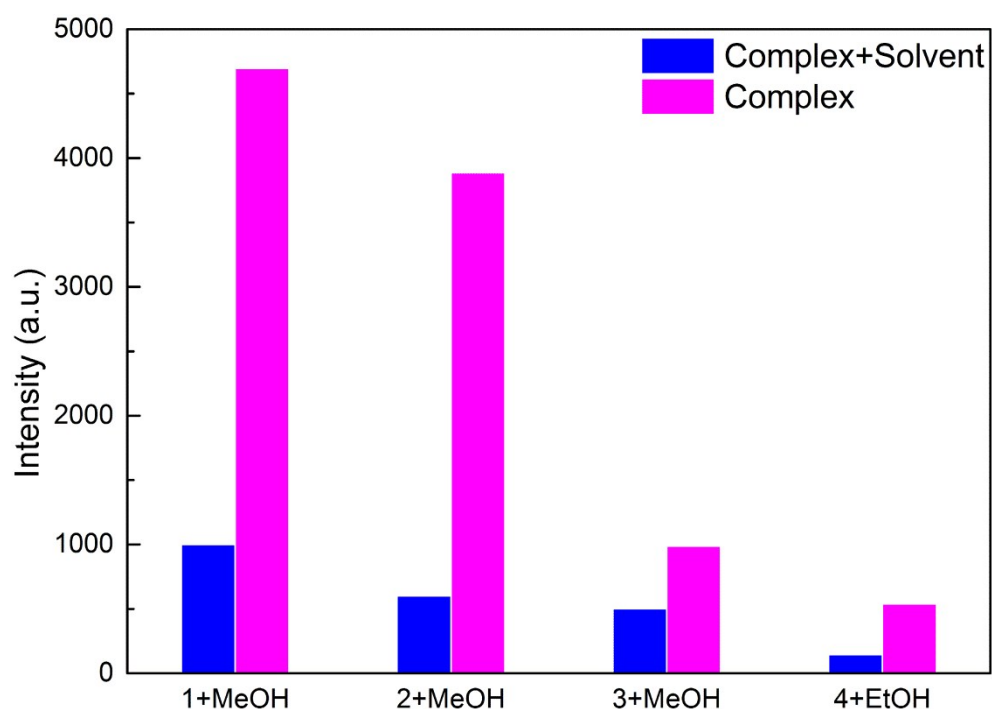


Fig. S17 Change of fluorescent emission intensity of complexes **1-4** from their solution state [$\lambda_{\text{exc}} = 445$ nm; 542 nm of **1** (2.5×10^{-5} mol L⁻¹), 556 nm of **2** (2.5×10^{-5} mol L⁻¹), 563 nm of **3** (2.5×10^{-5} mol L⁻¹), 582 nm of **4** (2.5×10^{-5} mol L⁻¹) (the blue bar)] to their solid state [$\lambda_{\text{exc}} = 385$ nm; 568 nm of **1**, 589 nm of **2**, 595 nm of **3**, 634 nm of **4** (the pink bar)]. The selected solutions are those from which crystal state **1-4** were obtained.

9. DFT and TD-DFT Computations of the ligands of complexes **1**, **2**, **3** and **4**

DFT and TD-DFT calculations were performed using the Gaussian 09 suite of programs.^[1] Geometry optimizations and vertical excitations of Ligand **L1**, **L2**, **L3** and **L4** were obtained at the B3LYP/6-31G* level of theory.

For **1**, the absorbance band around 407 nm is dominated by the HOMO → LUMO excitation, the details of the vertical excitation energies, oscillator strengths, and excitations nature are shown in Table S1.

Table S12. TD-DFT calculated electronic transition configurations for **L1**, **L2**, **L3**, and **L4** along with their corresponding excitation energies and oscillator strengths

Compound	Spin State	Transition Configuration	Excitation	Oscillator
			Energy (nm, eV)	Strength
1	S1	HOMO → LUMO (98%)	407(3.05)	0.1847
	S2	HOMO-1 → LUMO (96%)	400(3.10)	0.0709
	S3	HOMO-2 → LUMO (88%)	376(3.29)	0.1512
2	S1	HOMO → LUMO (99%)	411(3.01)	0.2086
	S2	HOMO-1 → LUMO (96%)	408(3.04)	0.0747
	S3	HOMO-2 → LUMO (23%) HOMO → LUMO+1 (68%)	387(3.20)	0.1495
3	S1	HOMO → LUMO (99%)	422(2.94)	0.161
	S2	HOMO-1 → LUMO (98%)	419(2.96)	0.0688
	S3	HOMO-3 → LUMO (10%) HOMO → LUMO+1 (88%)	401(3.09)	0.1088
4	S1	HOMO → LUMO (99%)	440(2.82)	0.1537
	S2	HOMO-1 → LUMO (98%)	425(2.92)	0.0770
	S3	HOMO → LUMO+1 (93%)	418(2.96)	0.1018

Table S13. Primary orbitals which contribute to the calculated transitions of **L1** (iso = 0.03).

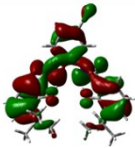
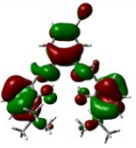
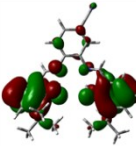
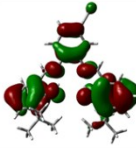
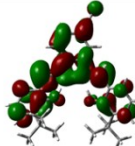
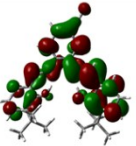
HOMO-4	HOMO-2	HOMO-1	HOMO
			
LUMO	LUMO+1		
			

Table S14. Primary orbitals which contribute to the calculated transitions of **L2** (iso = 0.03).

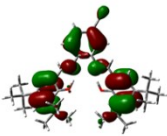
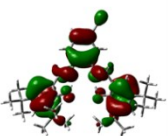
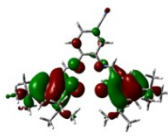
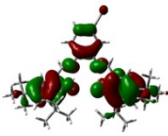
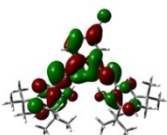
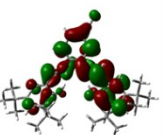
HOMO-3	HOMO-2	HOMO-1	HOMO
			
LUMO	LUMO+1		
			

Table S15. Primary orbitals which contribute to the calculated transitions of **L3** (iso = 0.03).

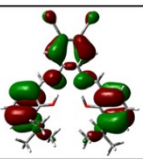
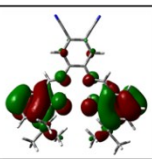
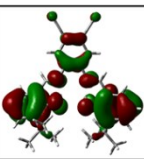
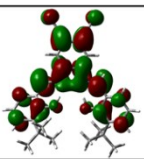
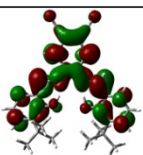
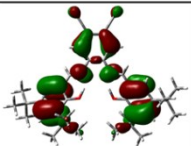
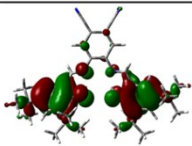
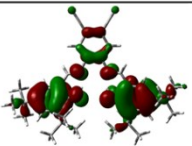
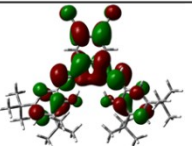
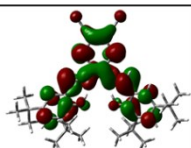
HOMO-3	HOMO-1	HOMO	LUMO
			
LUMO+1			
			

Table S16. Primary orbitals which contribute to the calculated transitions of **L4** (iso = 0.03).

HOMO-3	HOMO-1	HOMO	LUMO
			
LUMO+1			
			

10. UV-vis titration of complexes **1**, **2**, **3** and **4** with F⁻, Cl⁻ and Br⁻ in THF

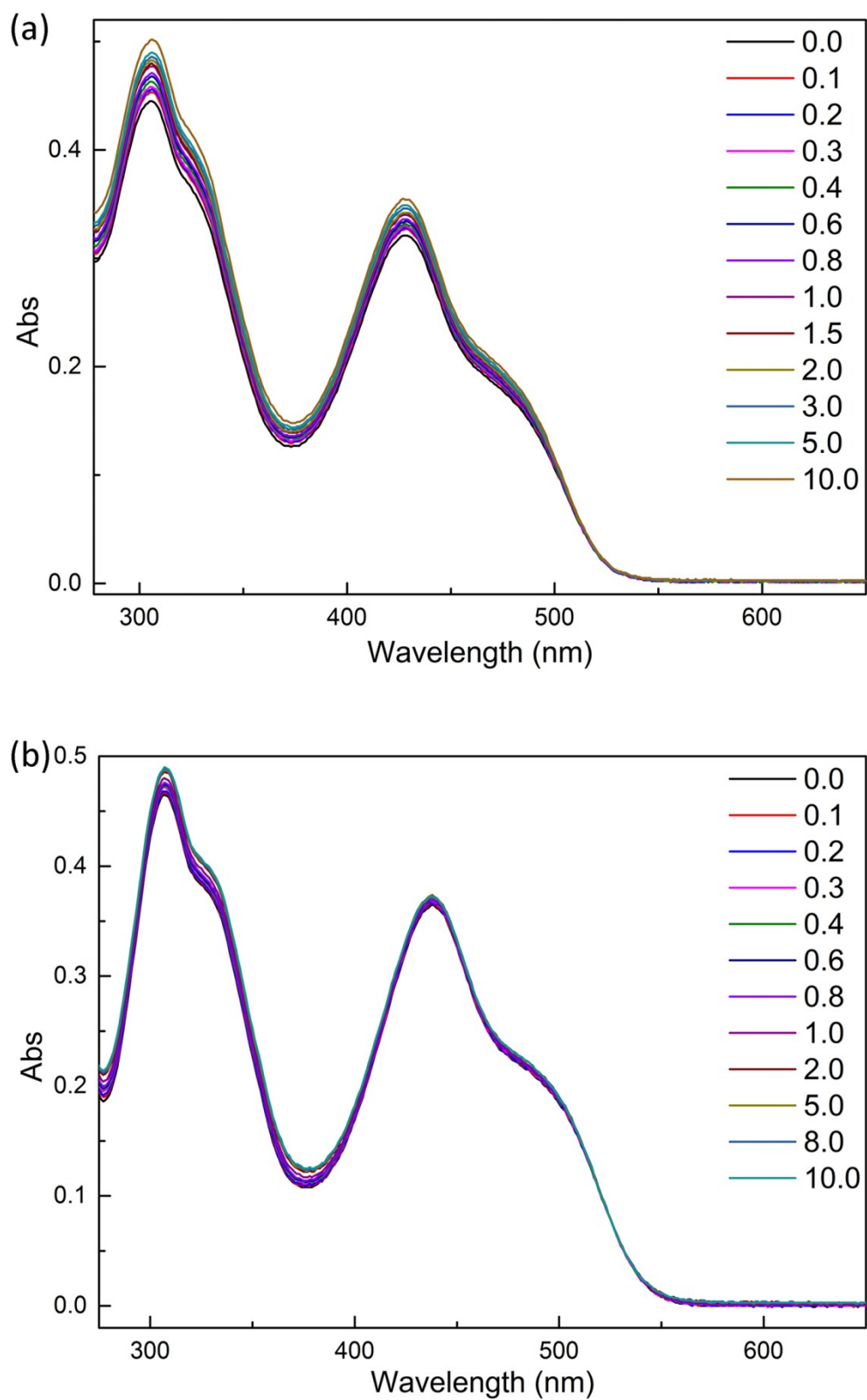


Fig. S18 UV-Vis spectra of **1** and **2** upon titration of NaF in THF. (a) **1** (2.5×10^{-5} mol L⁻¹), NaF (0-10 eq); (b) **2** (2.5×10^{-5} mol L⁻¹), NaF (0-10 eq).

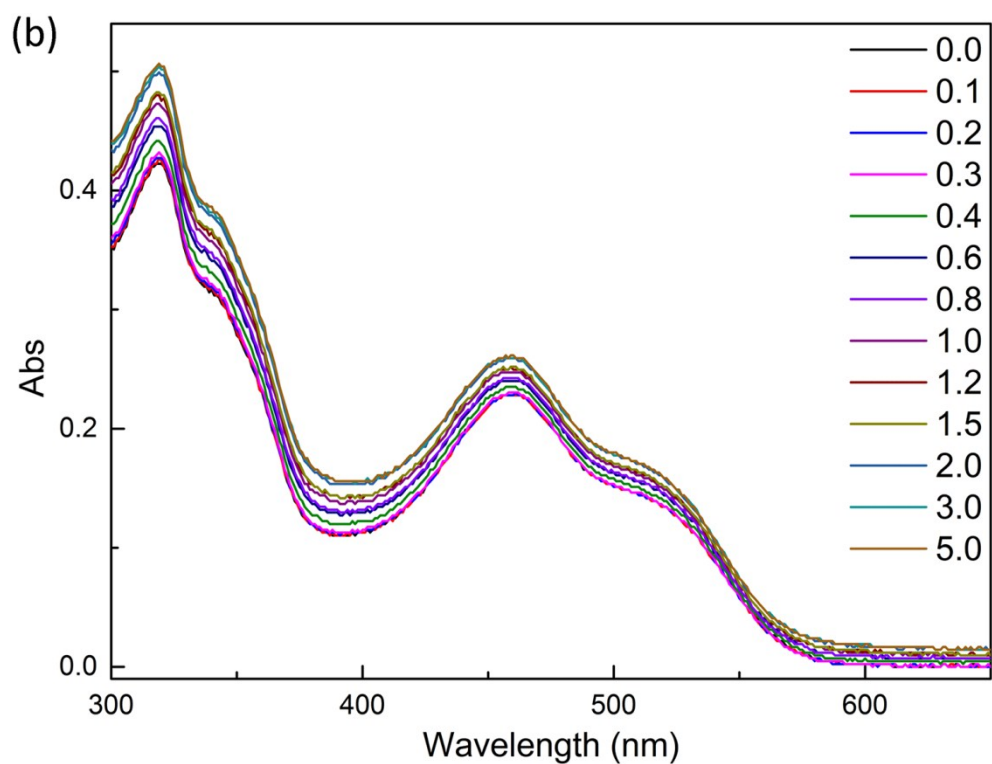
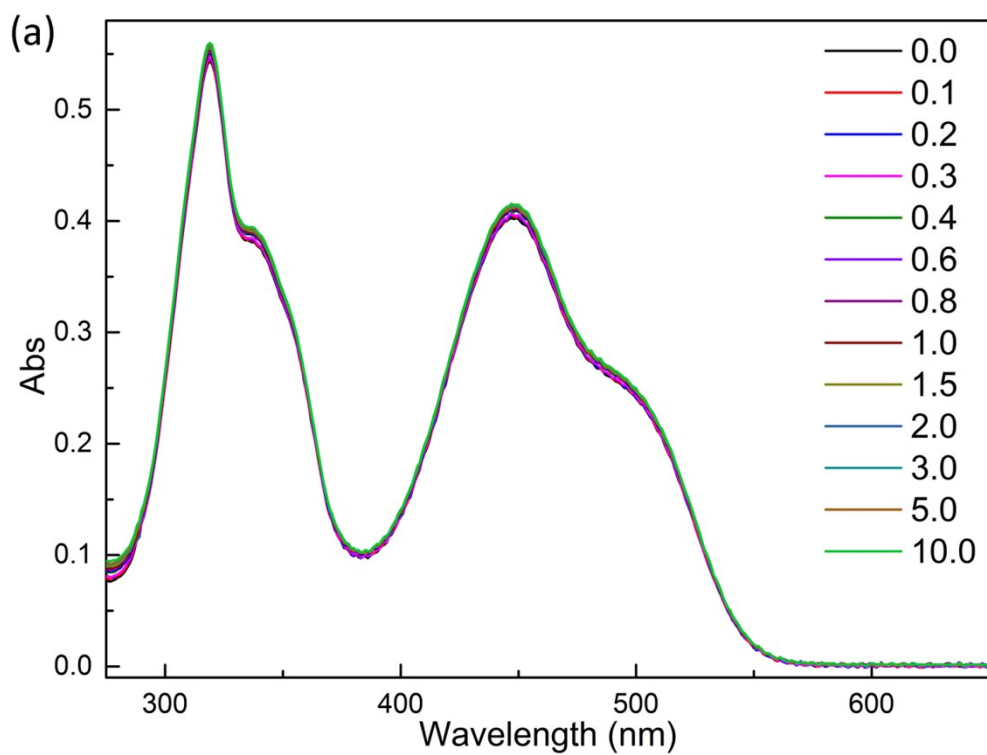


Fig. S19 UV-Vis spectra of **3** and **4** upon titration of NaF in THF. (a) **3** (2.5×10^{-5} mol L⁻¹), NaF (0-10 eq); (b) **4** (2.5×10^{-5} mol L⁻¹), NaF (0-10 eq).

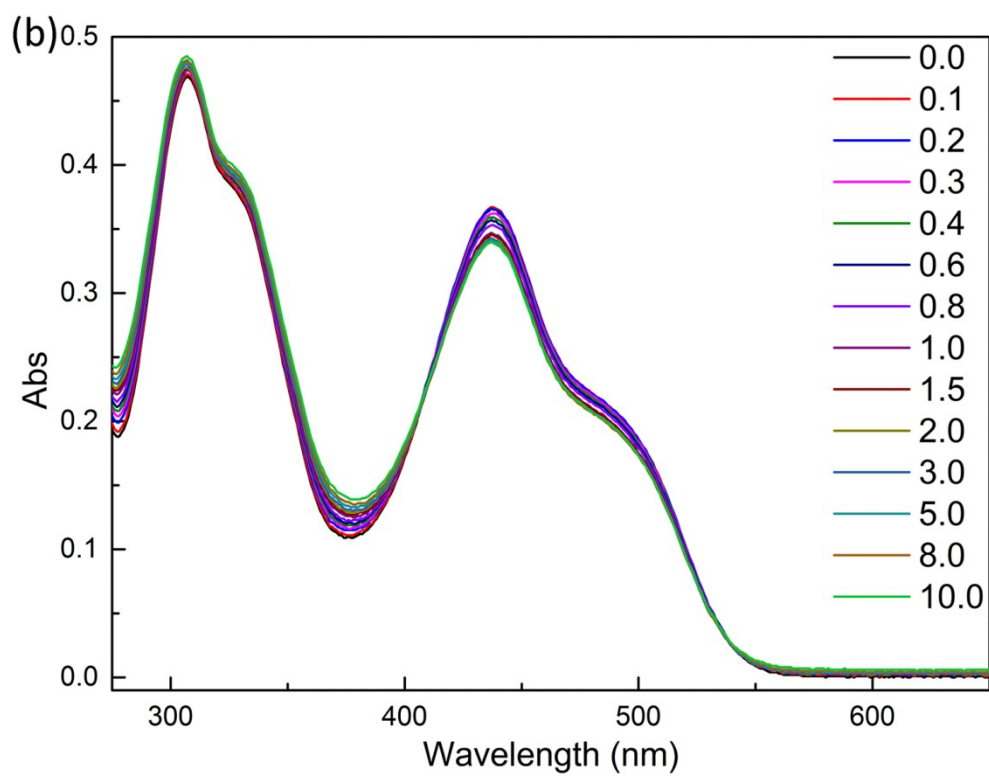
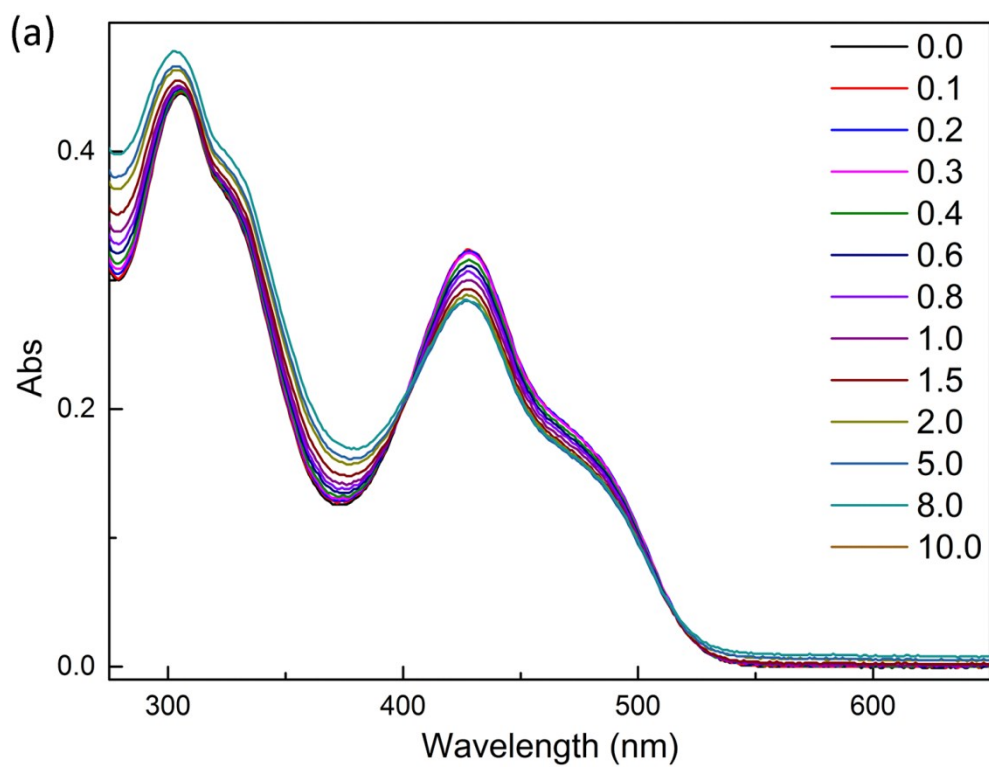


Fig. S20 UV-vis spectra of **1** and **2** upon titration of NaCl in THF. (a) **1** ($2.5 \times 10^{-5} \text{ mol L}^{-1}$), NaCl (0-10 eq); (b) **2** ($2.5 \times 10^{-5} \text{ mol L}^{-1}$), NaCl (0-10 eq).

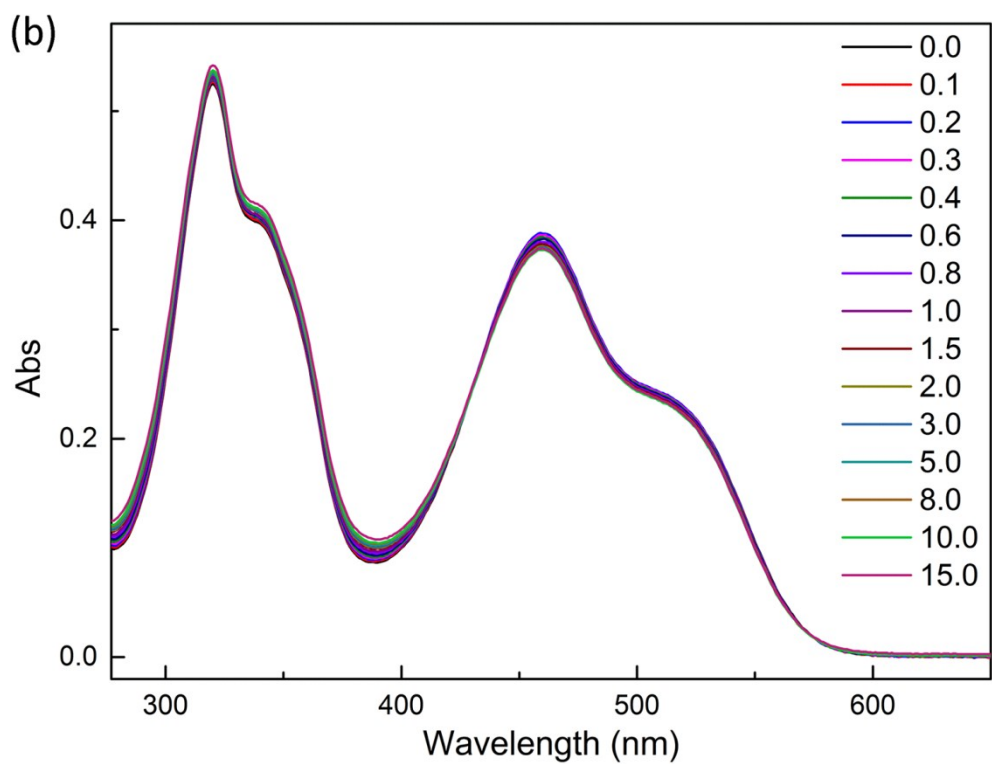
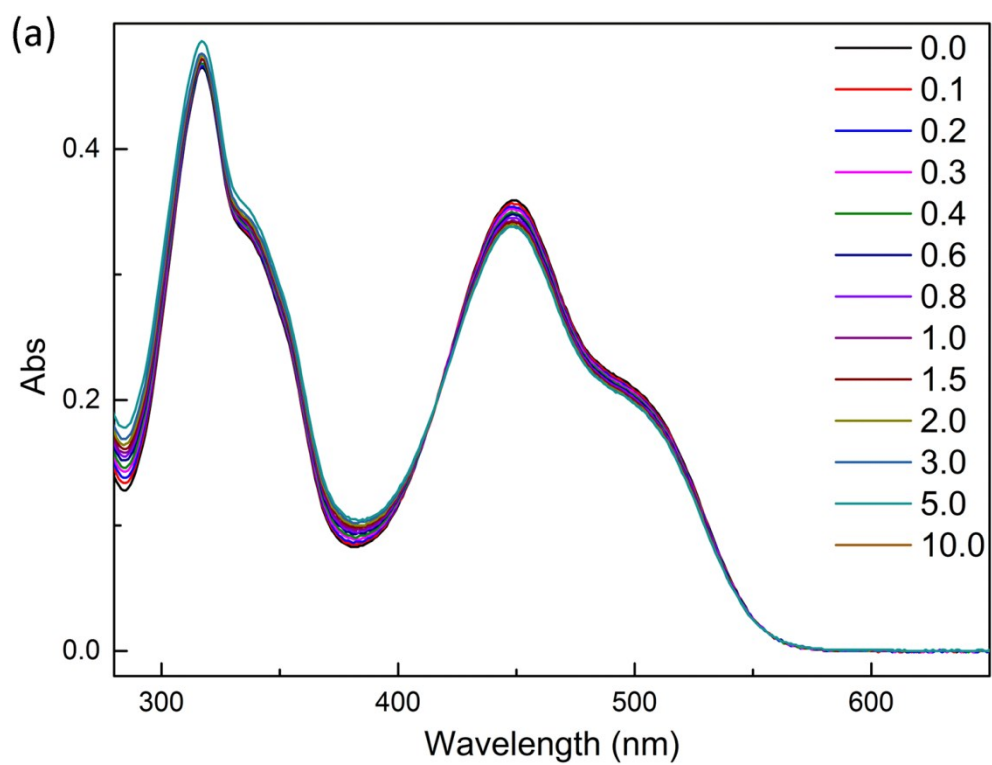


Fig. S21 UV-vis spectra of **3** and **4** upon titration of NaCl in THF. (a) **3** (2.5×10^{-5} mol L⁻¹), NaCl (0-10 eq); (b) **4** (2.5×10^{-5} mol L⁻¹), NaCl (0-10 eq).

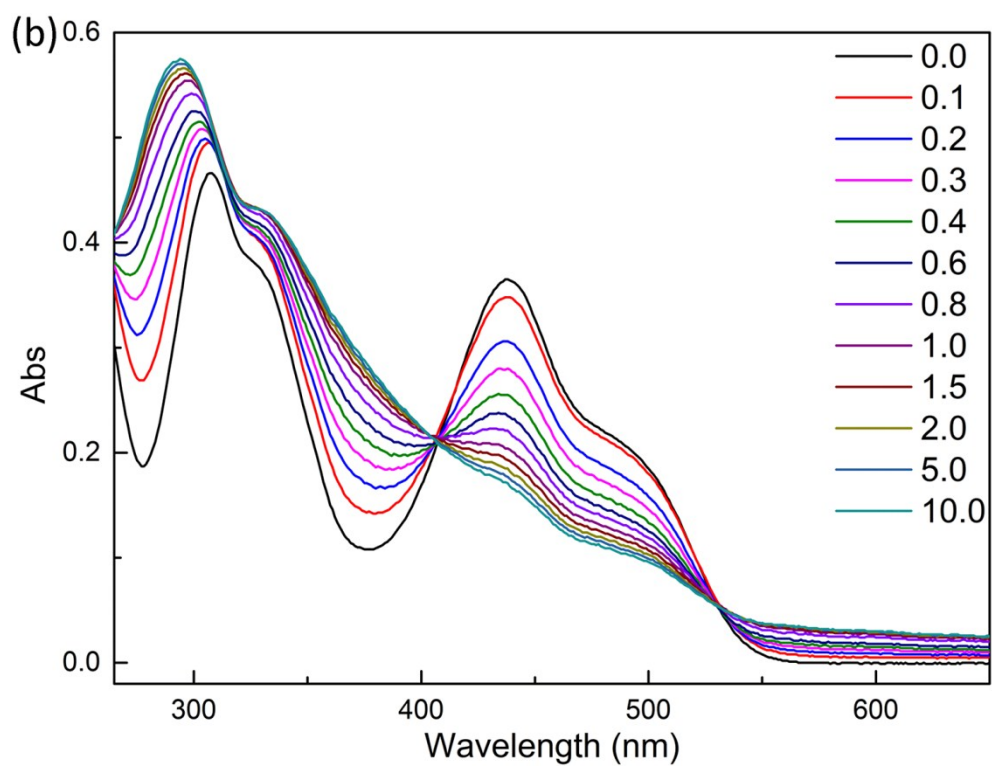
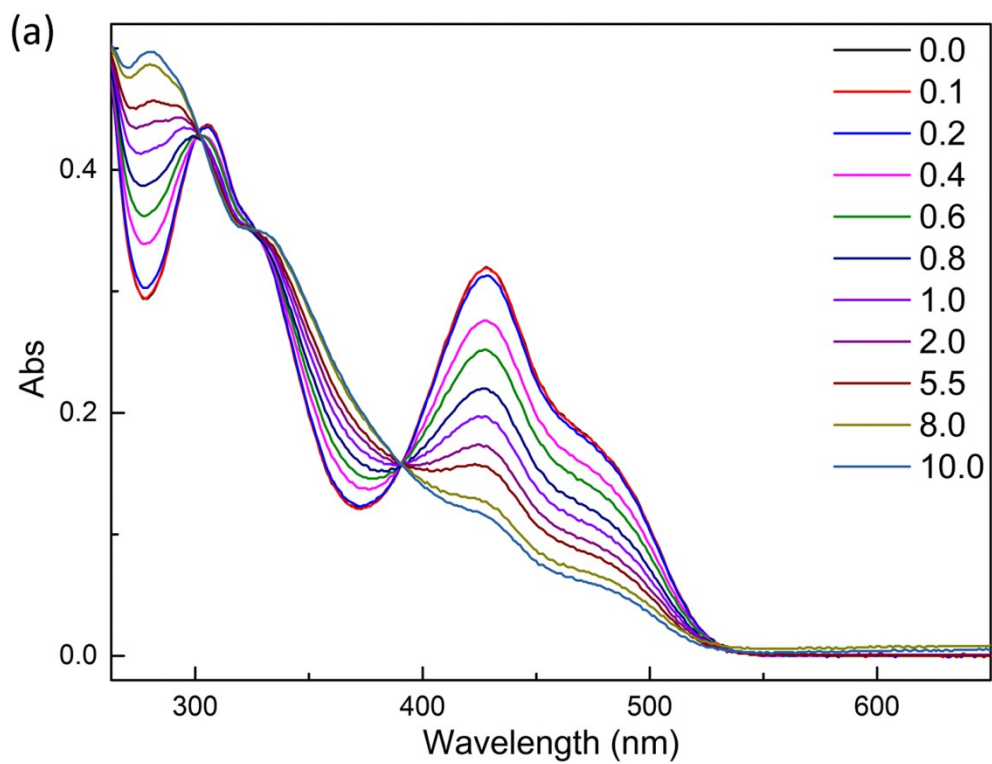


Fig. S22 UV-vis spectra of **1** and **2** upon titration of NaBr in THF. (a) **1** (2.5×10^{-5} mol L⁻¹), NaBr (0-10 eq); (b) **2** (2.5×10^{-5} mol L⁻¹), NaBr (0-10 eq).

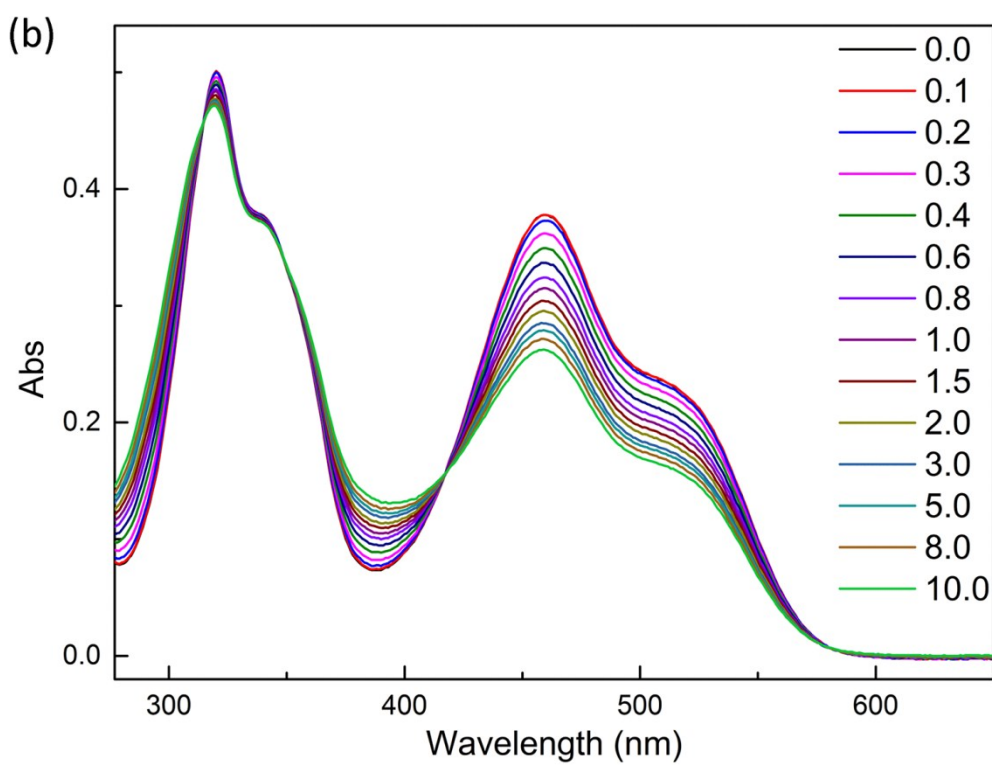
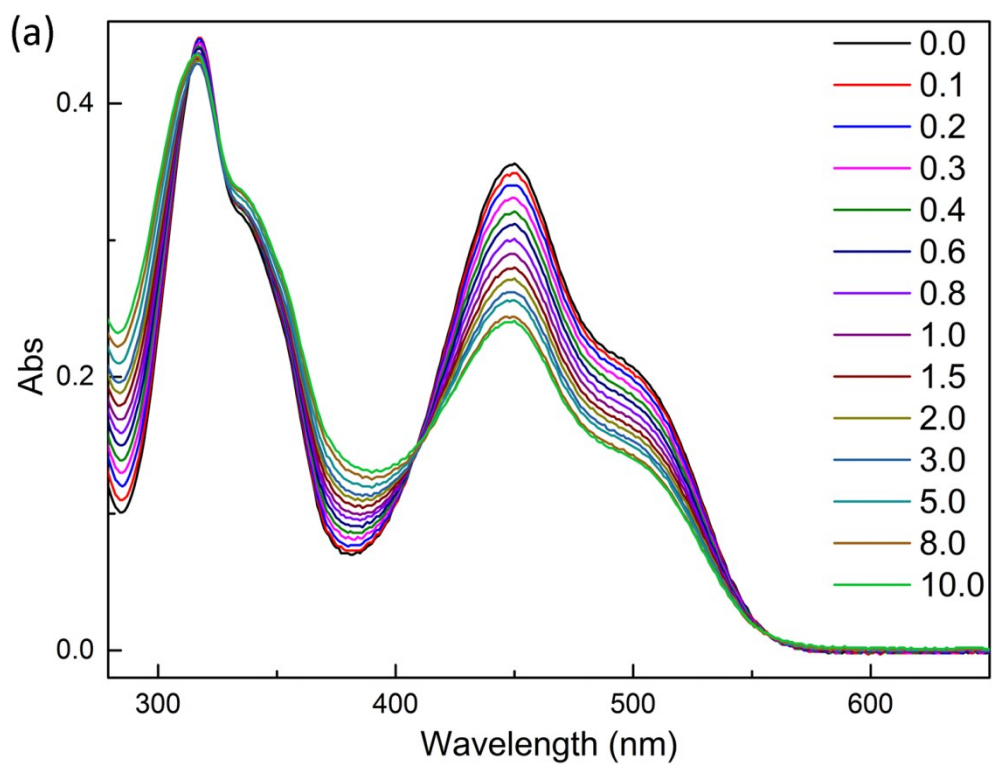


Fig. S23 UV-vis spectra of **3** and **4** upon titration of NaBr in THF. (a) **3** ($2.5 \times 10^{-5} \text{ mol L}^{-1}$), NaBr (0-10 eq); (b) **4** ($2.5 \times 10^{-5} \text{ mol L}^{-1}$), NaBr (0-10 eq)..

11. Fluorescence titration of complexes **1**, **2**, **3** and **4** with F⁻, Cl⁻ and Br⁻ in THF

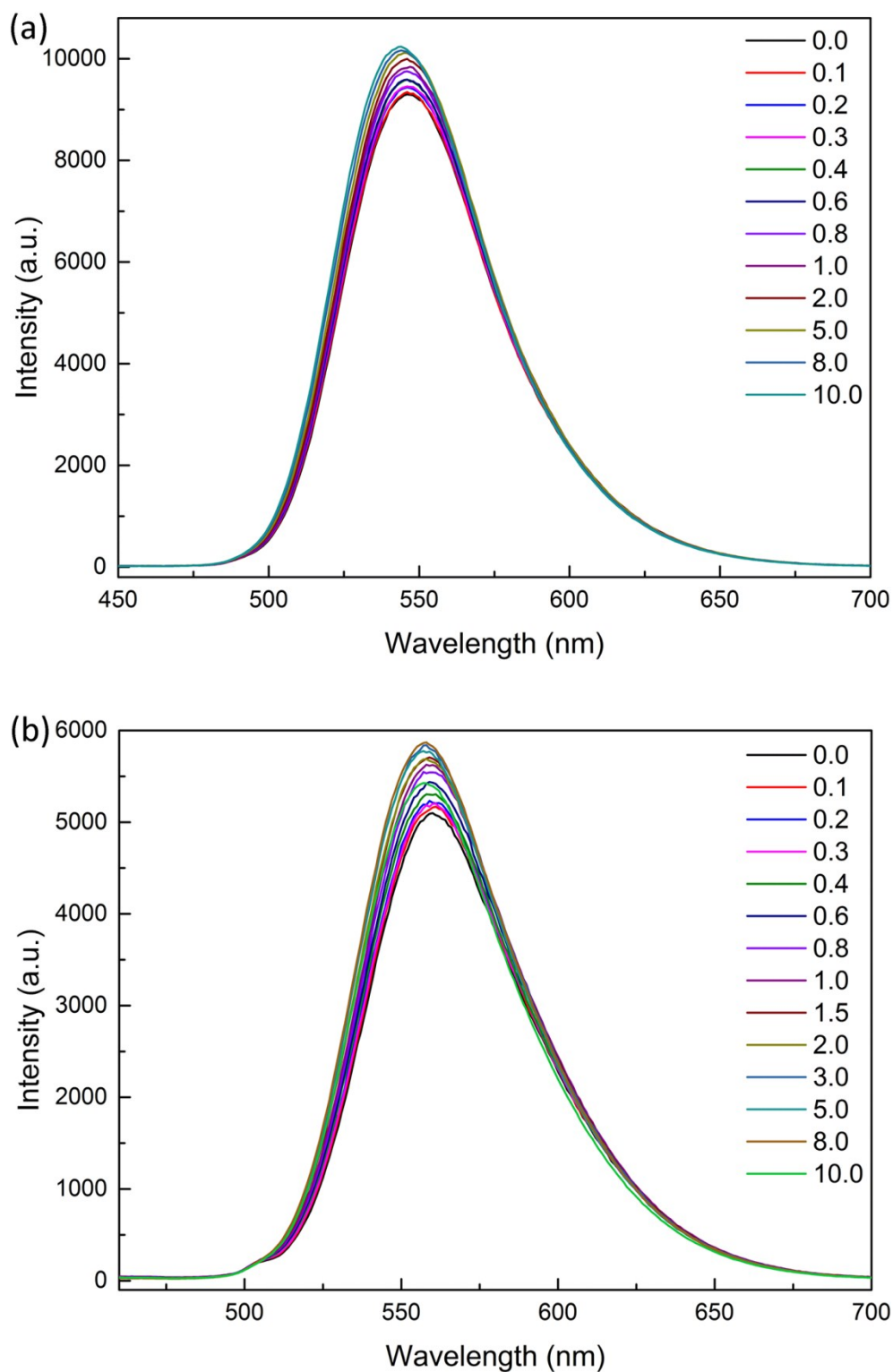


Fig. S24 Fluorescence spectra ($\lambda_{\text{exc}} = 445 \text{ nm}$) of **1** and **2** upon titration of NaF in THF. (a) **1** ($2.5 \times 10^{-5} \text{ mol L}^{-1}$), NaF (0-10 eq); (b) **2** ($2.5 \times 10^{-5} \text{ mol L}^{-1}$), NaF (0-10 eq).

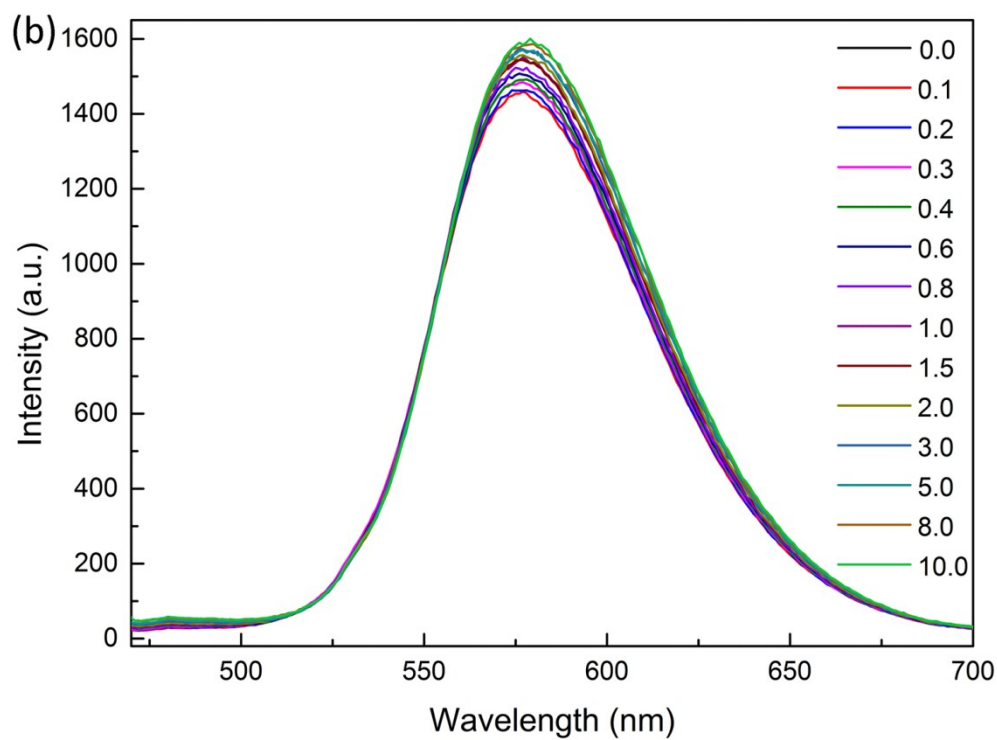
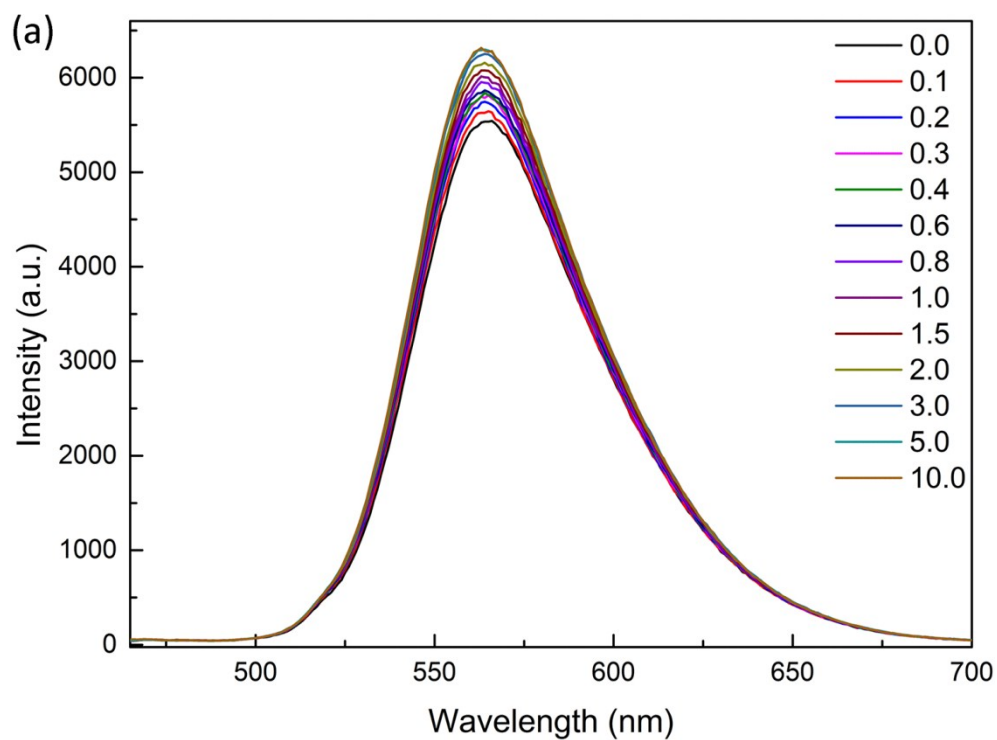


Fig. S25 Fluorescence spectra ($\lambda_{\text{exc}} = 445 \text{ nm}$) of **3** and **4** upon titration of NaF in THF. (a) **3** ($2.5 \times 10^{-5} \text{ mol L}^{-1}$), NaF (0-10 eq); (b) **4** ($2.5 \times 10^{-5} \text{ mol L}^{-1}$), NaF (0-10 eq).

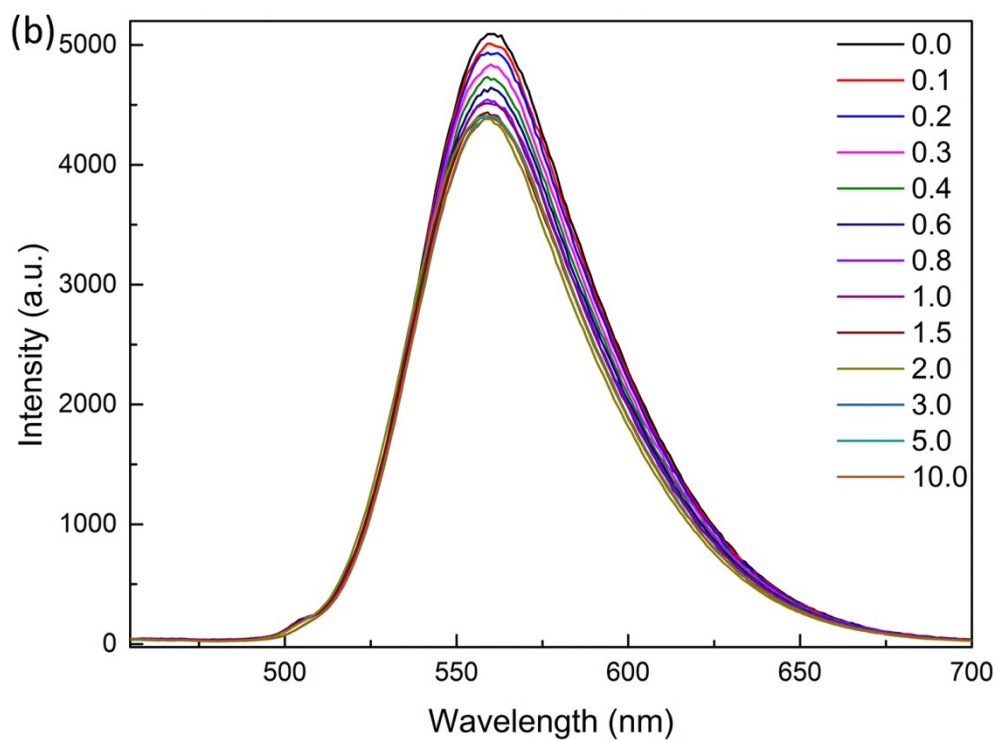
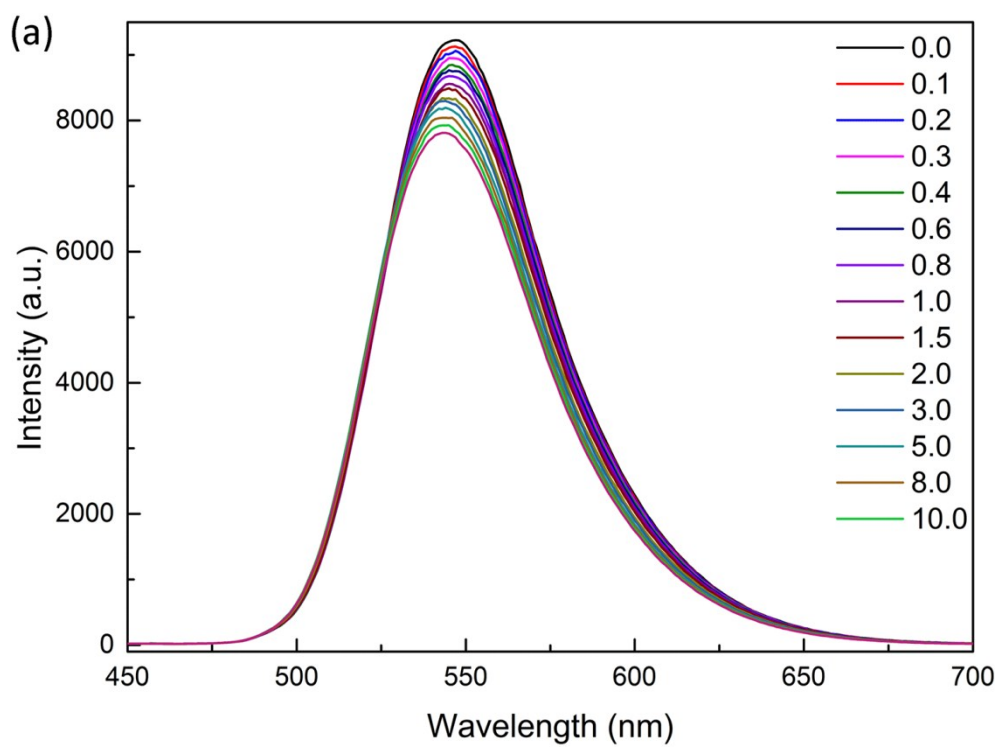


Fig. S26 Fluorescence spectra ($\lambda_{\text{exc}} = 445 \text{ nm}$) of **1** and **2** upon titration of NaCl in THF. (a) **1** ($2.5 \times 10^{-5} \text{ mol L}^{-1}$), NaCl (0-10 eq); (b) **2** ($2.5 \times 10^{-5} \text{ mol L}^{-1}$), NaCl (0-10 eq).

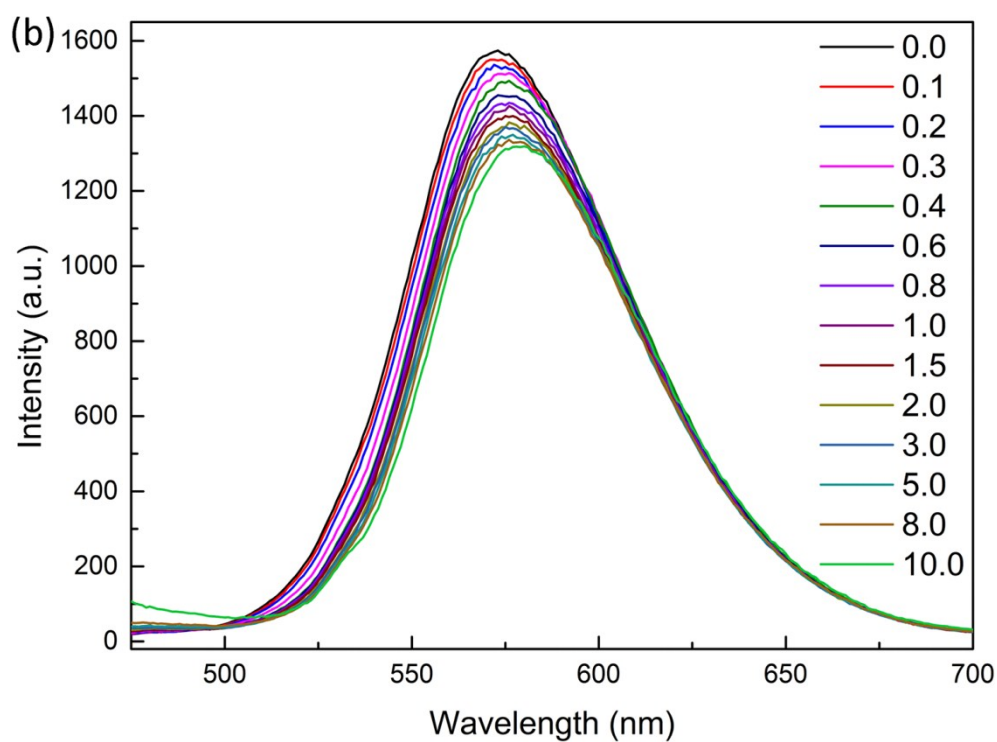
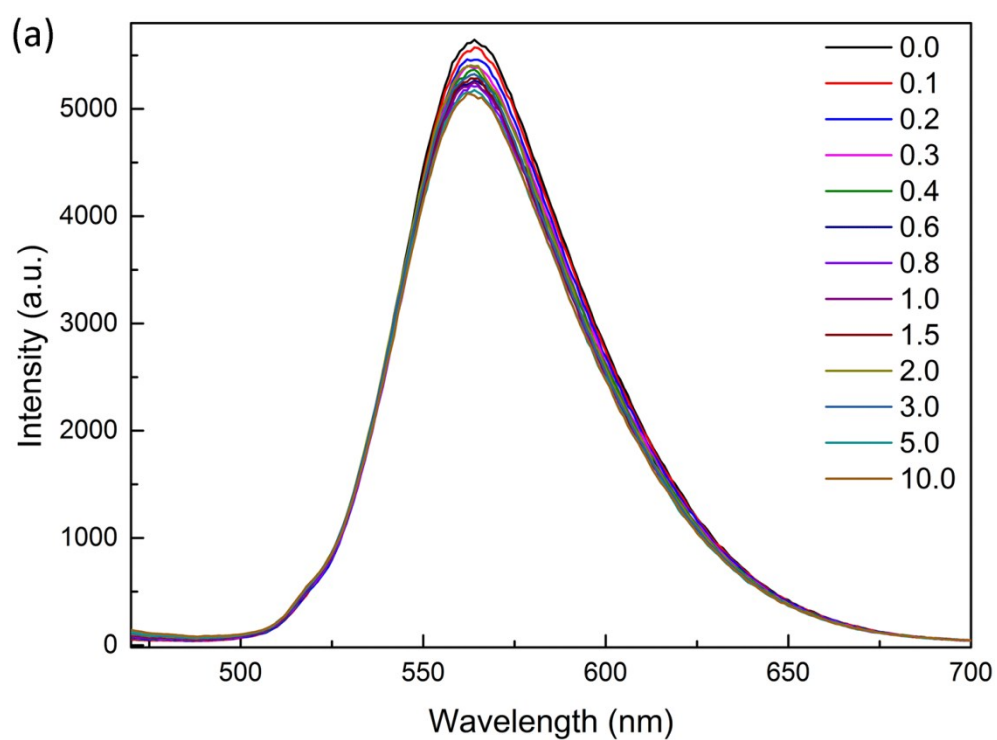


Fig. S27 Fluorescence spectra ($\lambda_{\text{exc}} = 445 \text{ nm}$) of **3** and **4** upon titration of NaCl in THF. (a) **3** ($2.5 \times 10^{-5} \text{ mol L}^{-1}$), NaCl (0-10 eq); (b) **4** ($2.5 \times 10^{-5} \text{ mol L}^{-1}$), NaCl (0-10 eq).

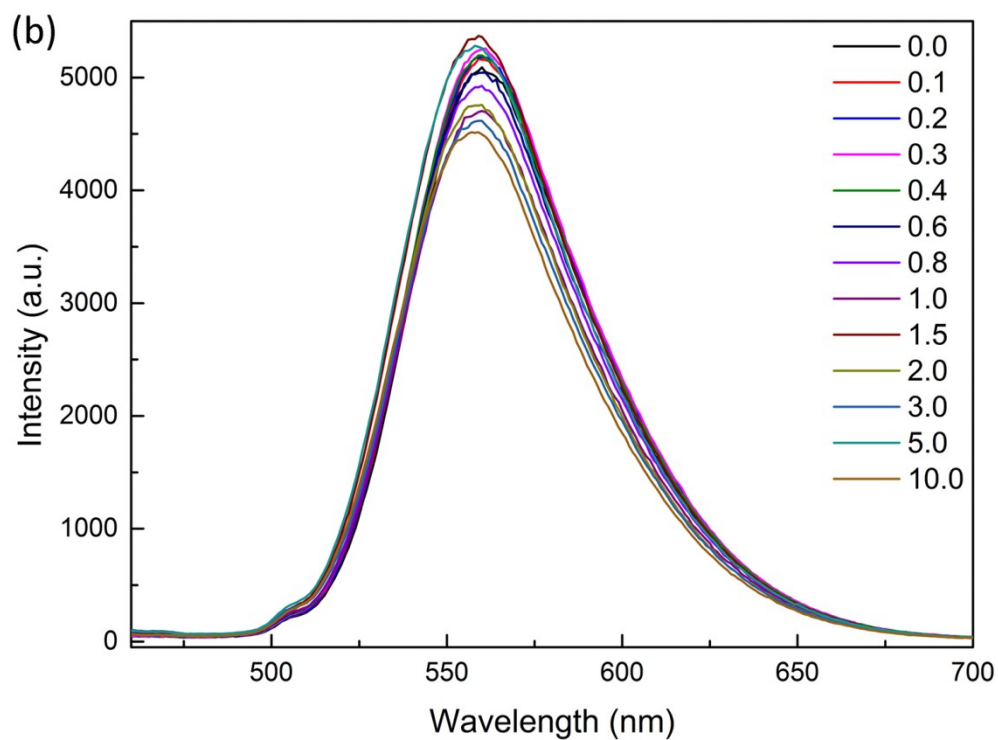
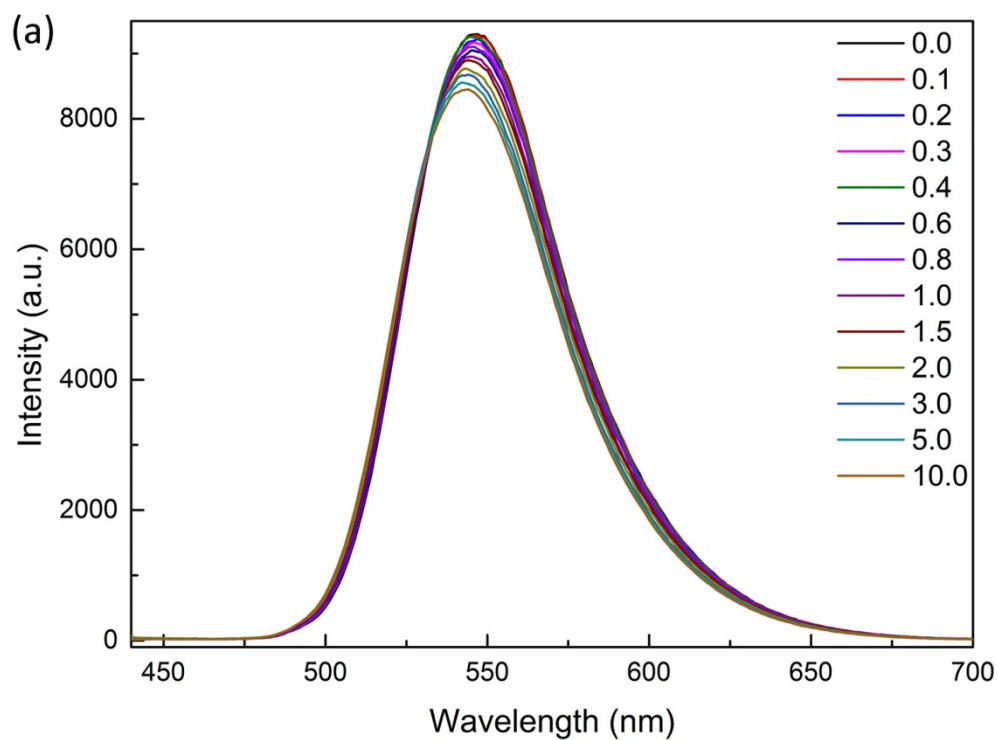


Fig. S28 Fluorescence spectra ($\lambda_{\text{exc}} = 445 \text{ nm}$) of **1** and **2** upon titration of NaBr in THF. (a) **1** ($2.5 \times 10^{-5} \text{ mol L}^{-1}$), NaBr (0-10 eq); (b) **2** ($2.5 \times 10^{-5} \text{ mol L}^{-1}$), NaBr (0-10 eq).

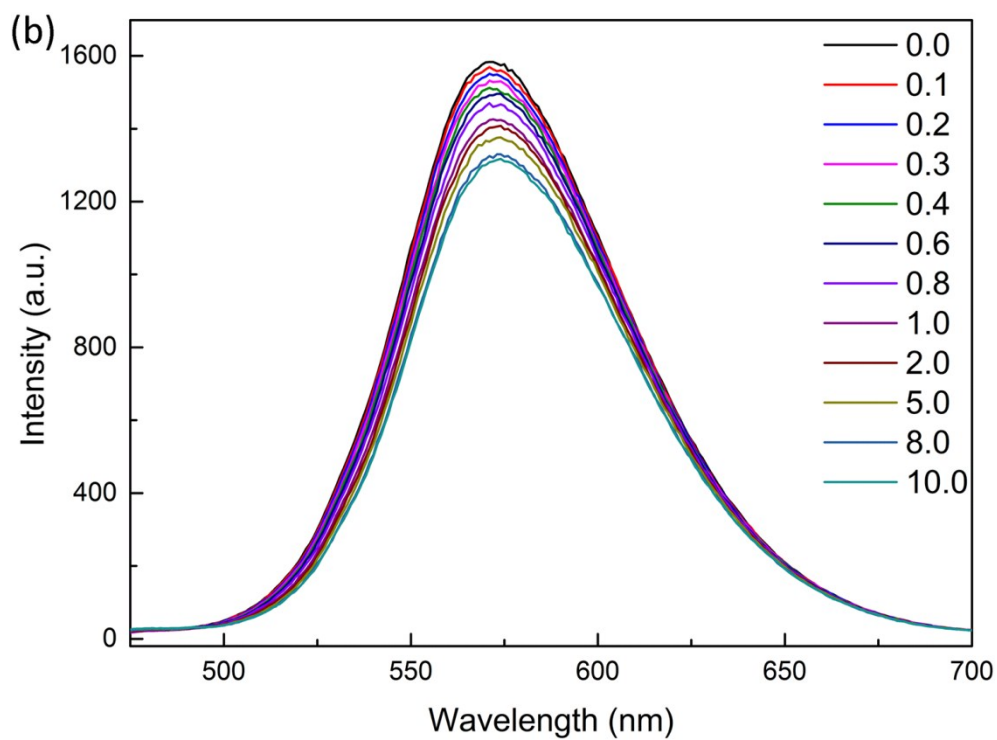
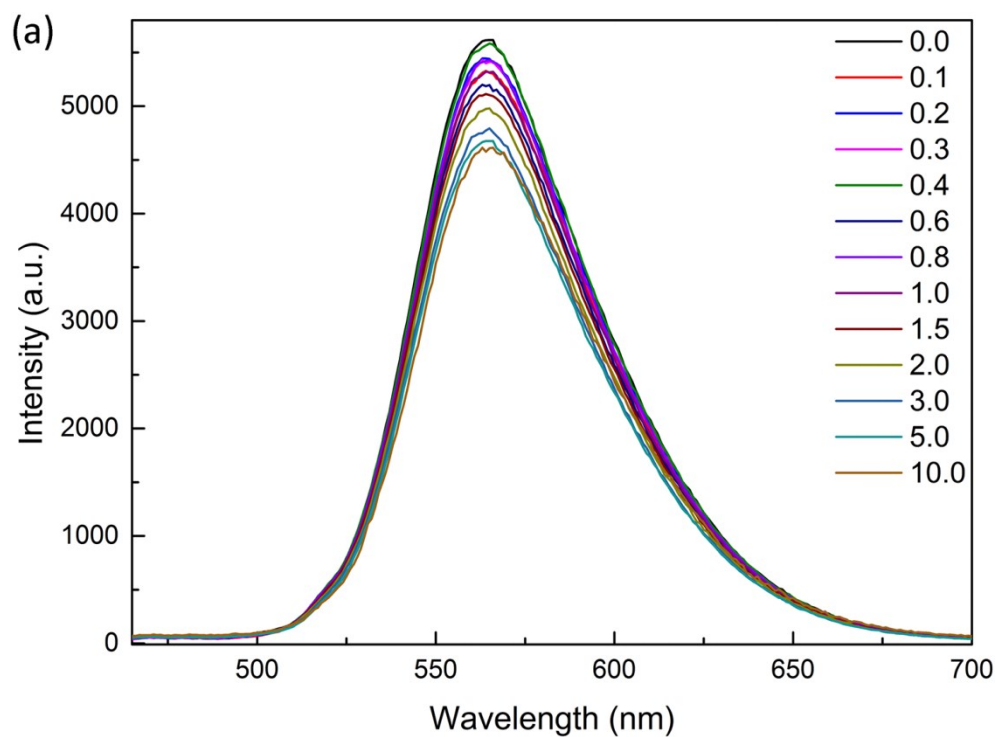


Fig. S29 Fluorescence spectra ($\lambda_{\text{exc}} = 445 \text{ nm}$) of **3** and **4** upon titration of NaBr in THF. (a) **3** ($2.5 \times 10^{-5} \text{ mol L}^{-1}$), NaBr (0-10 eq); (b) **4** ($2.5 \times 10^{-5} \text{ mol L}^{-1}$), NaBr (0-10 eq).

12. Iodide recognition of complexes **1**, **2**, **3** and **4** in THF

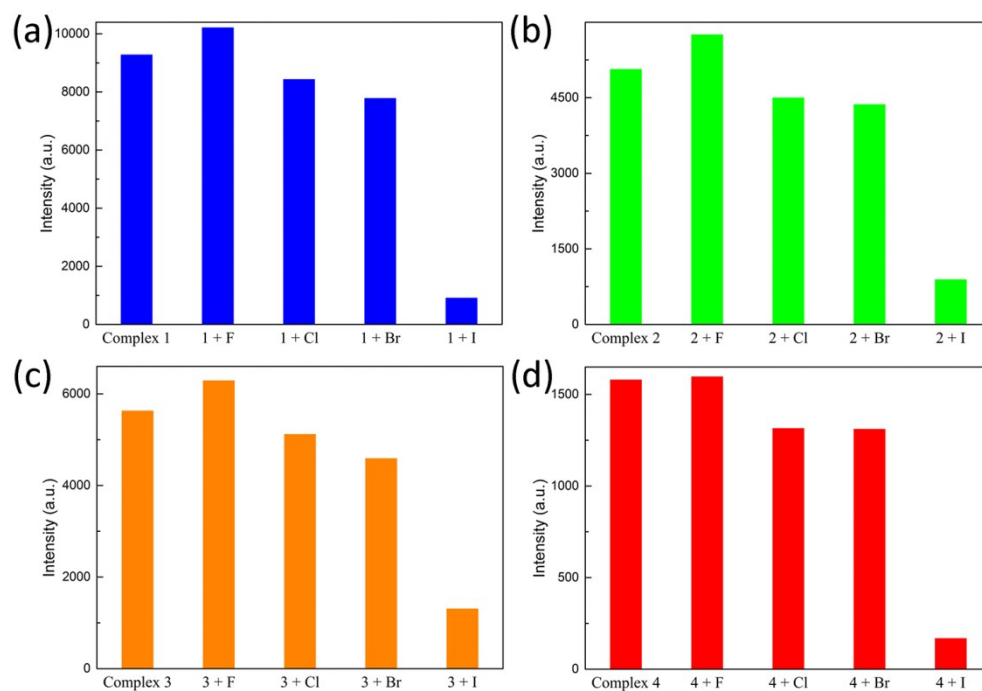


Fig. S30 (a) Bar graph of Change of fluorescent emission intensities ($\lambda_{\text{ex}}=445$ nm) at (a) 542 nm of **1** (2.5×10^{-5} mol L⁻¹), (b) 556 nm of **2** (2.5×10^{-5} mol L⁻¹), (c) 563 nm of **3** (2.5×10^{-5} mol L⁻¹), (d) 582 nm of **4** (2.5×10^{-5} mol L⁻¹) on addition of 10 equiv. of F⁻, Cl⁻, Br⁻ and I⁻ respectively in THF.

13. Benesi-Hilderbrand and Job's plot curve of complexes 1, 2, 3 and 4 with I⁻ monitored with UV-Vis spectra

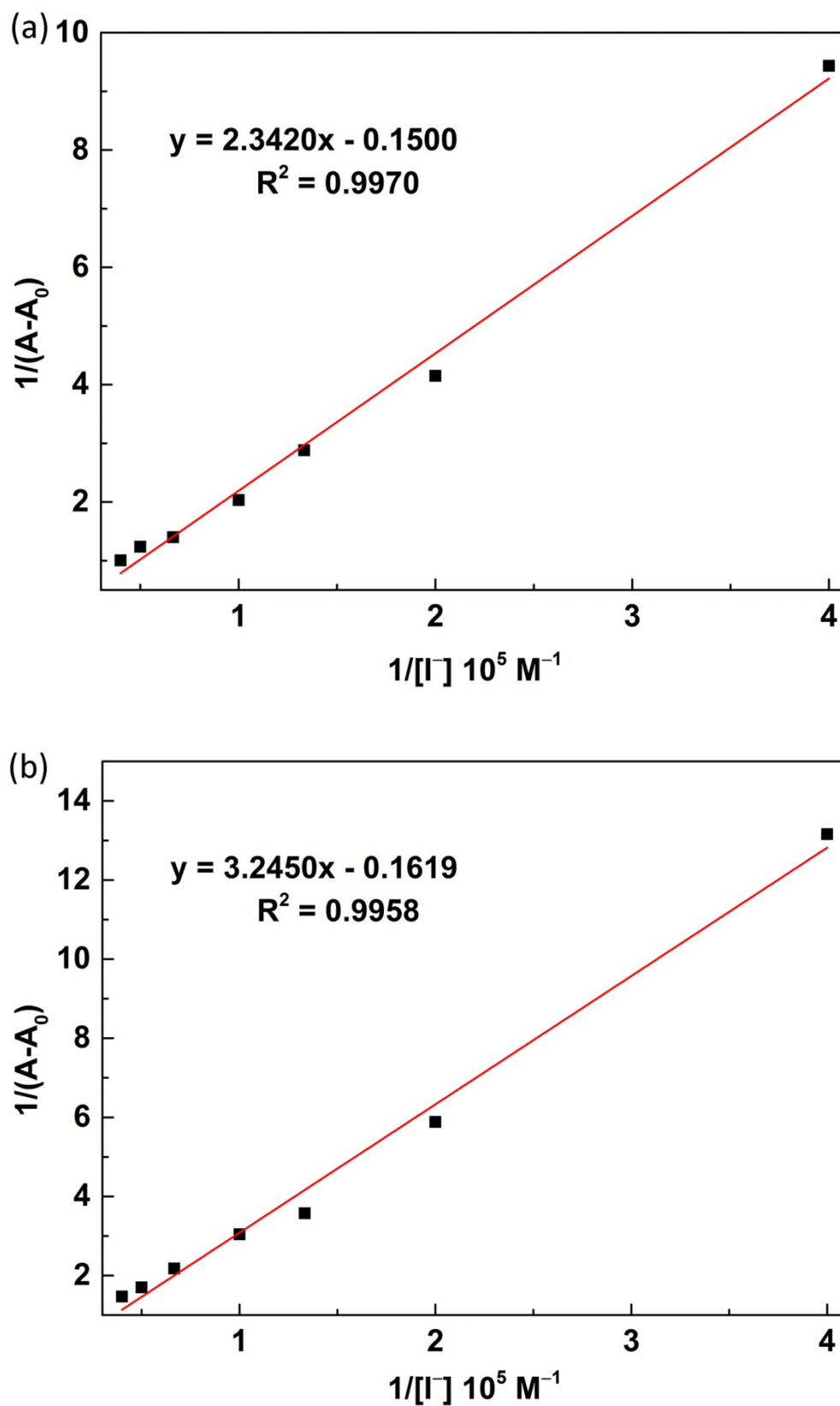


Fig. S31 The Benesi-Hilderbrand curve of complexes 1 (a) and 2 (b) for I⁻.

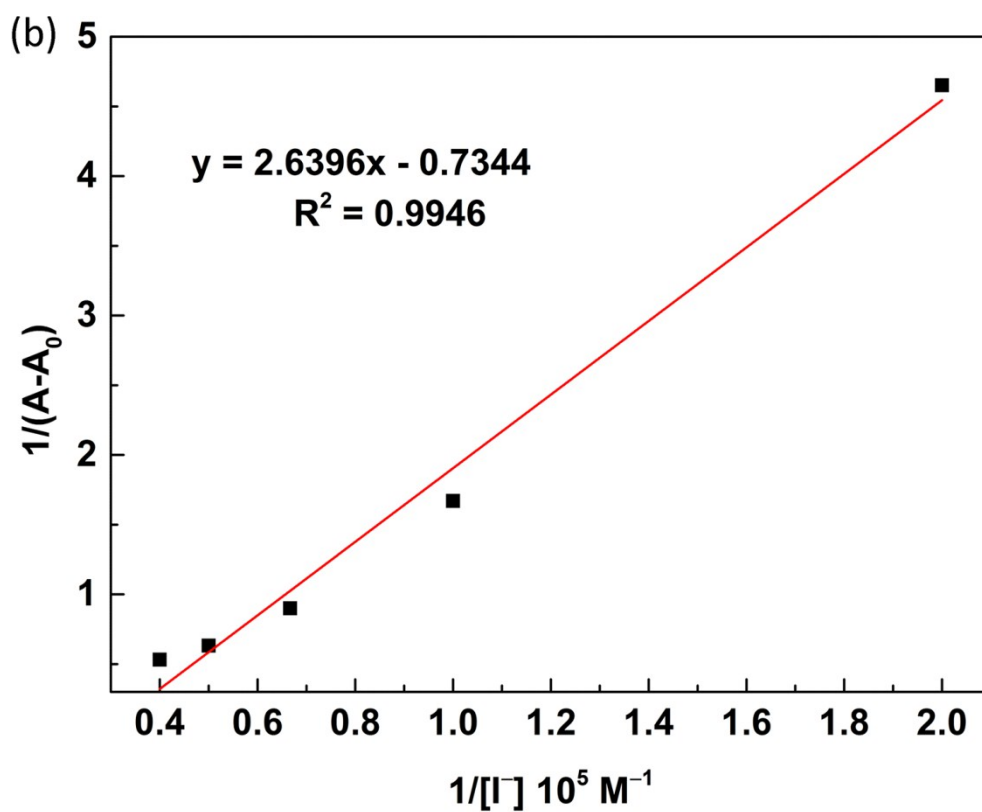
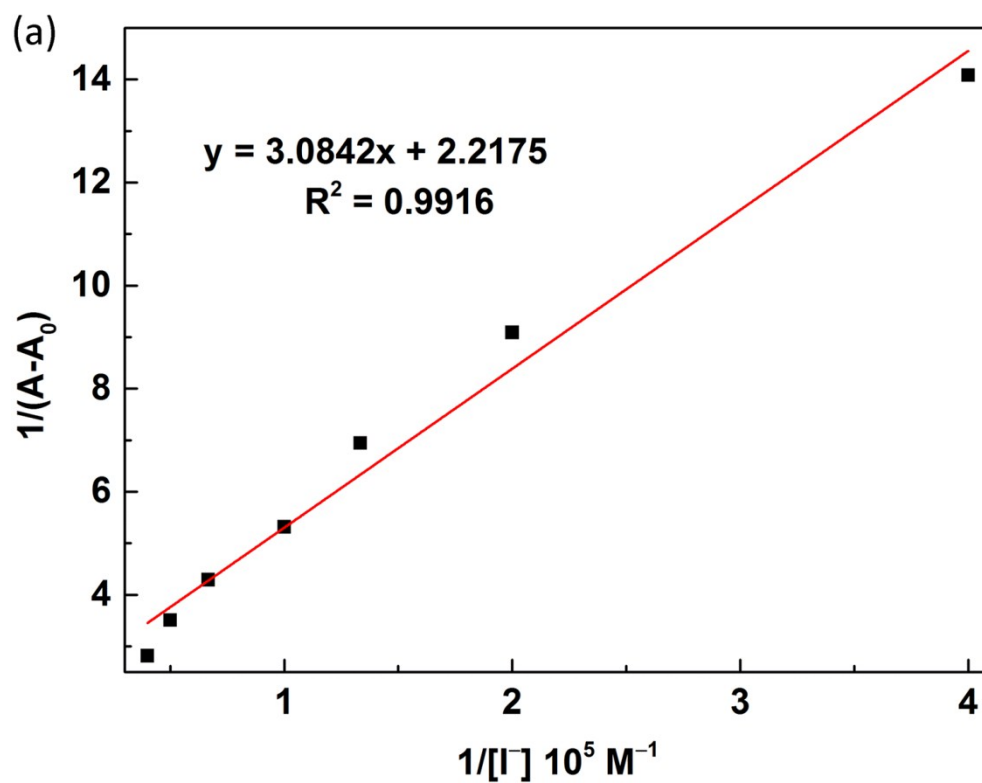


Fig. S32 The Benesi-Hildebrand curve of complexes **1** (a) and **2** (b) for I.

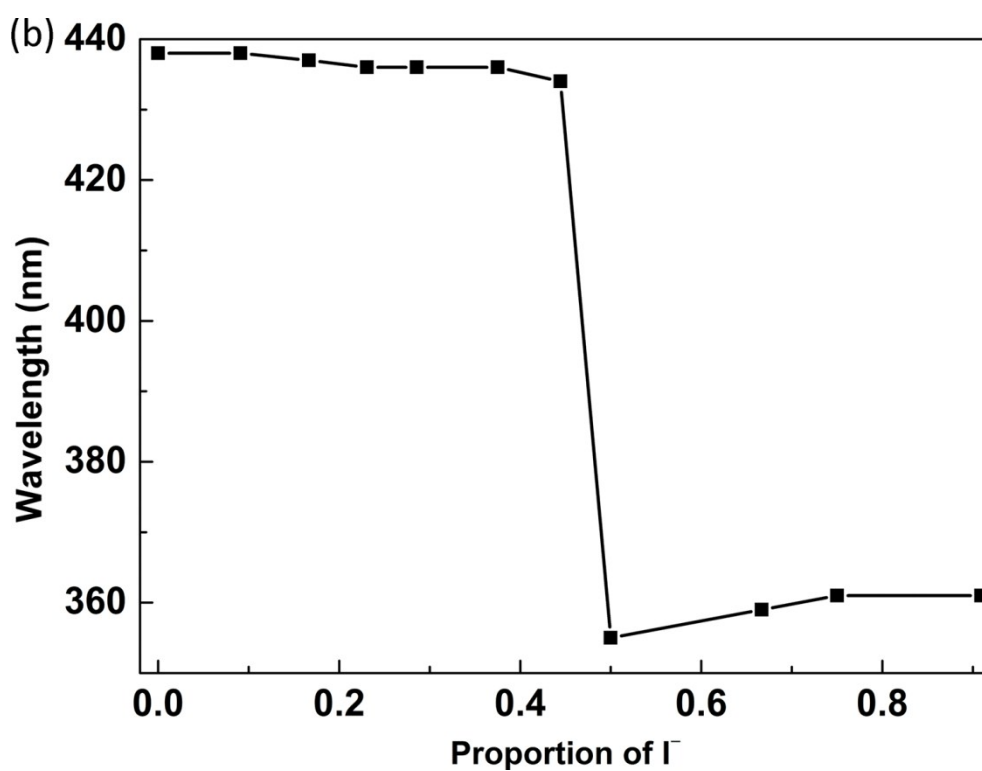
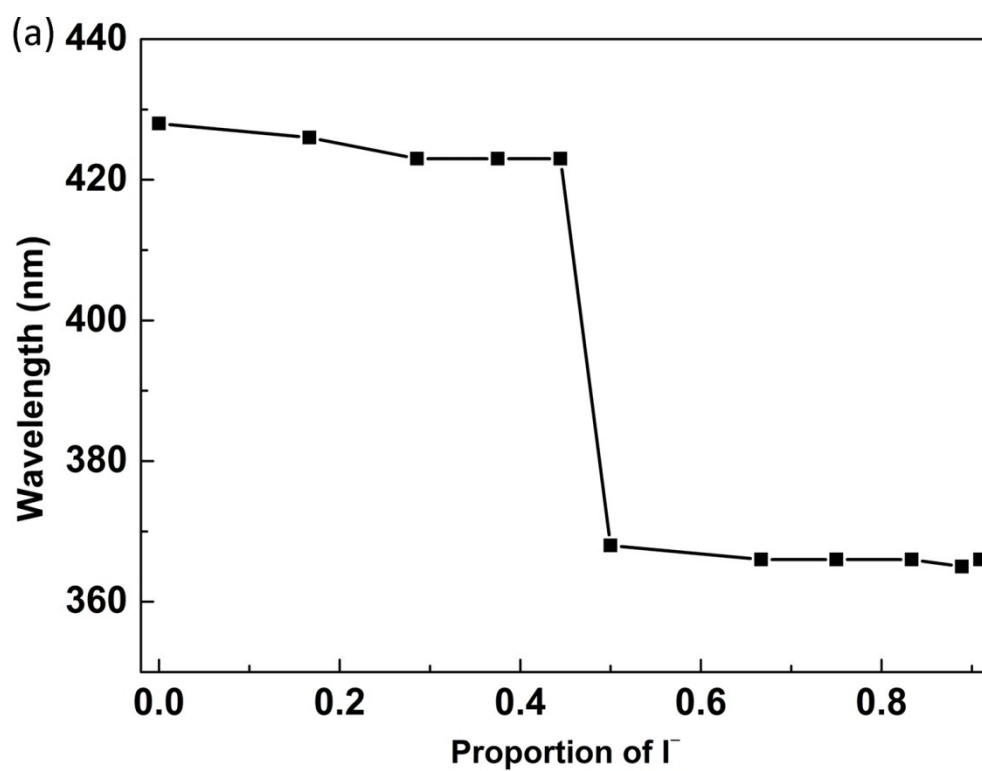


Fig. S33 Job's plot of the complex formation of **1** (a) and **2** (b) with I⁻ monitored with UV/vis spectra.

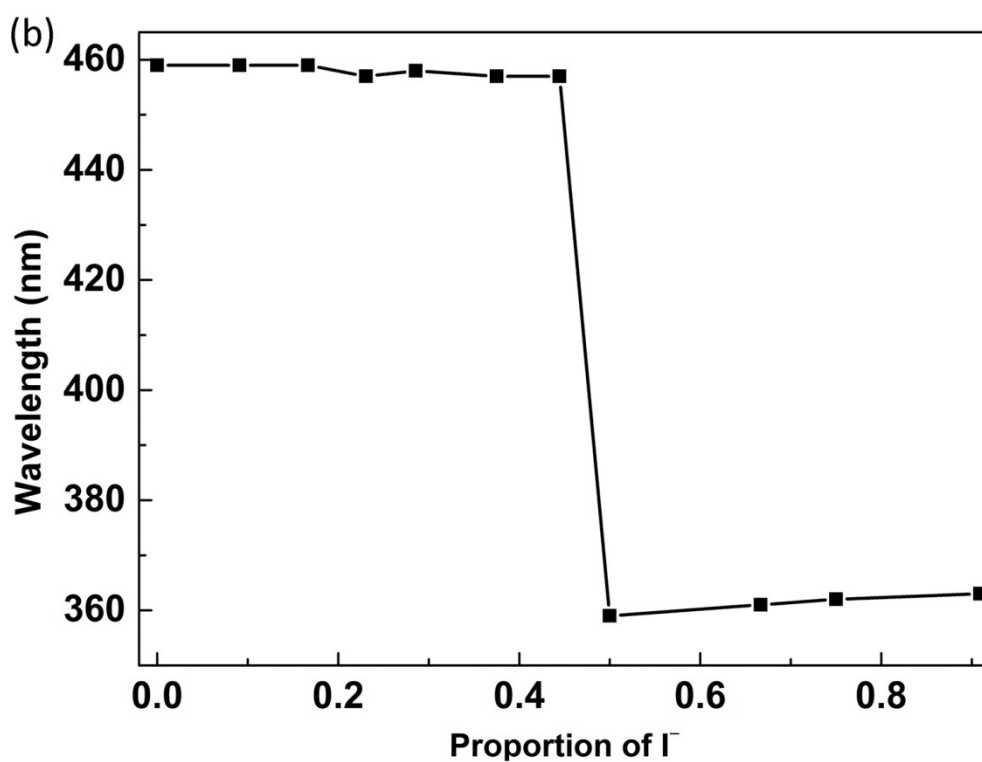
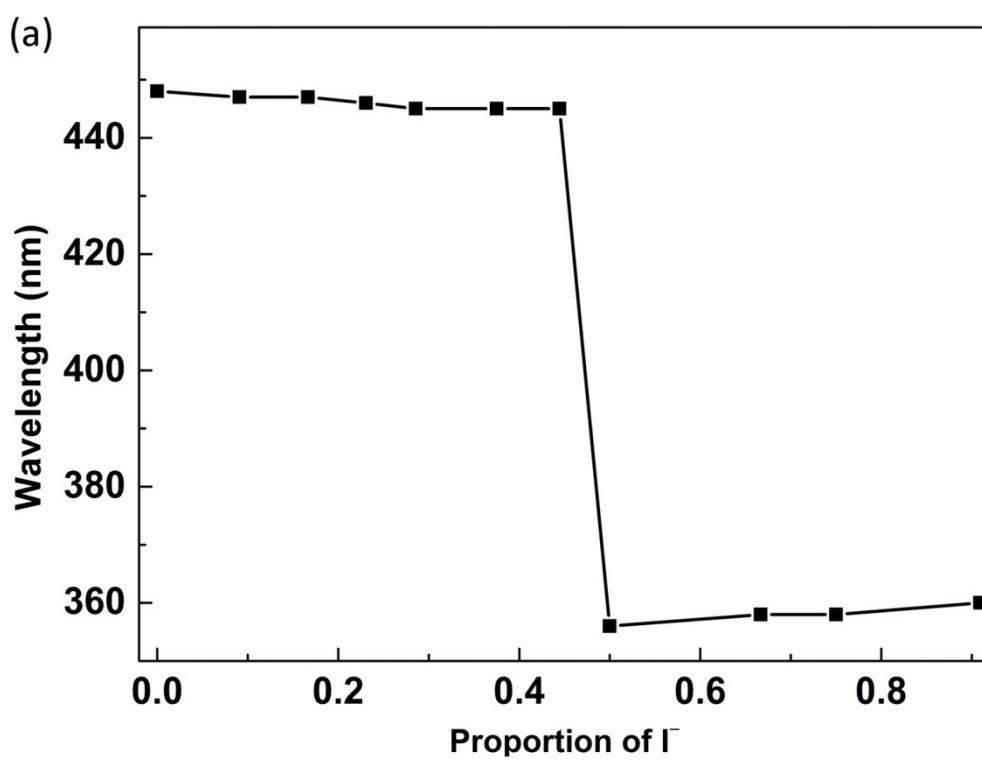


Fig. S34 Job's plot of the complex formation of **3** (a) and **4** (b) with I^- monitored with UV/vis spectra.

References:

[1] M. J. Frisch, G. W. Trucks, H. B. Schlegel, G. E. Scuseria, M. A. Robb, J. R. Cheeseman, G. Scalmani, V. Barone, B. Mennucci, G. A. Petersson, H. Nakatsuji, M. Caricato, X. Li, H. P. Hratchian, A. F. Izmaylov, J. Bloino, G. Zheng, J. L. Sonnenberg, M. Hada, M. Ehara, K. Toyota, R. Fukuda, J. Hasegawa, M. Ishida, T. Nakajima, Y. Honda, O. Kitao, H. Nakai, T. Vreven, J. A. Montgomery, Jr., J. E. Peralta, F. Ogliaro, M. Bearpark, J. J. Heyd, E. Brothers, K. N. Kudin, V. N. Staroverov, R. Kobayashi, J. Normand, K. Raghavachari, A. Rendell, J. C. Burant, S. S. Iyengar, J. Tomasi, M. Cossi, N. Rega, J. M. Millam, M. Klene, J. E. Knox, J. B. Cross, V. Bakken, C. Adamo, J. Jaramillo, R. Gomperts, R. E. Stratmann, O. Yazyev, A. J. Austin, R. Cammi, C. Pomelli, J. W. Ochterski, R. L. Martin, K. Morokuma, V. G. Zakrzewski, G. A. Voth, P. Salvador, J. J. Dannenberg, S. Dapprich, A. D. Daniels, O. Farkas, J. B. Foresman, J. V. Ortiz, J. Cioslowski, and D. J. Fox, Gaussian, Inc., Wallingford CT, 2009.